

Backdoor-based Explainable AI Benchmark for High Fidelity Evaluation of Attribution Methods

Peiyu Yang, Naveed Akhtar, Jiantong Jiang, and Ajmal Mian

Abstract—Attribution methods compute importance scores for input features to explain the output predictions of deep models. However, accurate assessment of attribution methods is challenged by the lack of benchmark fidelity for attributing model predictions. Moreover, other confounding factors in attribution estimation, including the setup choices of post-processing techniques and explained model predictions, further compromise the reliability of the evaluation. In this work, we first identify a set of fidelity criteria that reliable benchmarks for attribution methods are expected to fulfill, thereby facilitating a systematic assessment of attribution benchmarks. Next, we introduce a Backdoor-based eXplainable AI benchmark (BackX) that adheres to the desired fidelity criteria. We theoretically establish the superiority of our approach over the existing benchmarks for well-founded attribution evaluation. With extensive analysis, we also identify a setup for a consistent and fair benchmarking of attribution methods across different underlying methodologies. This setup is ultimately employed for a comprehensive comparison of existing methods using our BackX benchmark. Finally, our analysis also provides guidance for defending against backdoor attacks with the help of attribution methods.

Index Terms—Explainable AI, feature attribution, evaluation benchmark, neural backdoor.



1 INTRODUCTION

DEEP learning models have made remarkable strides across diverse domains [1]–[3] owing to their capacity to learn intricate representations through numerous parameters. However, the extensive parameter scale that contributes to their success also renders these models less interpretable for their decisions, limiting their applicability in high-stake tasks [4], [5].

In an effort to provide explanations for model predictions, attribution methods [6]–[8] ascribe importance scores, referred to as attributions, to the input features. Benefiting from their theoretical foundations [8]–[10], attribution methods are extensively employed in explaining model predictions and establishing model trustworthiness [1], [11]–[13]. Nevertheless, despite their popularity, the assessment of attribution methods faces challenges given the lack of ground truth. Consequently, the evaluation often relies on alternative techniques such as the removal of input features or the addition of perturbations [14]–[17]. However, such methods lead to a phenomenon known as *input distribution shift* [18], which compromises the fidelity of the evaluation benchmarks. Conversely, efforts have also been made to conjure attribution ground truth by leveraging training annotations [19], [20], generative framework [21] and model Trojaning [22]. However, these methods still encounter challenges in rigorously delineating the attribution ground truth, which impedes their reliability.

In this article, we first provide a set of clear fidelity criteria that eXplainable Artificial Intelligence (XAI) benchmarks should adhere to. We argue that these benchmarks should ensure fidelity to both the explained model and the input, thereby satisfying both *functional mapping invariance* (§ 3.1-1) and *input distribution invariance* (§ 3.1-2). Moreover, we stress that attribution benchmarks should offer verifiable ground truth for attributions and sensitive metrics for evaluating them, which we refer to as *attribution verifiability* (§ 3.1-3) and *metric sensitivity* (§ 3.1-4), respectively. Our foundational criteria not only set a standard for benchmarking but also facilitate a clear assessment of the existing XAI benchmarks. We then propose a new XAI benchmark (BackX) for attribution methods based on backdoor attacks [23]–[25]. Backdoor attacks render a model sensitive to a specific trigger pattern to control their predictions. We propose to leverage this explicit control to systematically establish ground truth attributions for the model. With thorough analysis, we show that the proposed BackX benchmark is capable of offering a more desirable level of assurance for fulfilling the fidelity criteria over the existing benchmarks.

To maintain benchmark fidelity, attribution evaluation must also deal with other confounding factors related to explanation post-processing and the choice of model output used for the explanation. Different choices in this regard eventually yield distinct attributions [26]–[28]. Incidentally, these confounders have often led to the development of additional explanatory techniques designed to clarify the explanations themselves [27]–[29], which is counterproductive. There is currently a lack of effort in pursuing a consistent framework for attribution evaluation. Through our well-founded BackX benchmark, we reveal distinct properties of different attribution methods using different setup choices, guiding us to a consistent benchmarking setup across different types of attribution methods. To the best of our knowledge, our work is the first to suggest

- Peiyu Yang, Jiantong Jiang and Ajmal Mian are with The University of Western Australia, Crawley, WA, 6009, Australia. E-mail: {peiyu.yang@research., jiantong.jiang@research., ajmal.mian@}uwa.edu.au
- Naveed Akhtar is with The University of Melbourne, Grattan Street, Parkville Victoria, 3010, Australia. E-mail: naveed.akhtar1@unimelb.edu.au

This paper was produced by the IEEE Publication Technology Group. They are in Piscataway, NJ.

a consistent setup for different types of attribution methods. Using the identified setup, we eventually assess a range of attribution methods using various trigger controls for different manipulated models under diverse Trojaning techniques. A by-product of this comprehensive analysis is unearthing valuable guidance for defense against backdoor attacks using attribution methods. In summary, this article contributes along the following three key aspects.

- 1) It systematically analyzes the attribution benchmark fidelity to identify key criteria for providing reliable foundations to the evaluation of attribution benchmarks.
- 2) It proposes a backdoor-based XAI benchmark (BackX) for attribution methods. The benchmark leverages controllable attributions through model manipulation, fulfilling the identified fidelity criteria. Superior fidelity of this benchmark is established through theoretical analysis.
- 3) It establishes a consistent setup for a transparent assessment of different types of attribution methods, and performs extensive benchmarking of existing methods with BackX using this setup. In the process, it also offers interesting guidance for defending against backdoor attacks with the help of attribution methods.

2 RELATED WORK

2.1 Attribution Methods

To explain model predictions, attribution methods [6], [7] assign importance scores to input features. Deconvnet [7] and Guided Backpropagation [30] utilize deconvolution technique to compute feature importance. CAM [31] introduces global-average pooling during back-propagation, enhancing localization ability without resorting to deconvolution. GradCAM [32] builds on CAM, improving generalization without introducing additional structures. Compared to CAM-based methods, InputGrad [6] calculates gradients with respect to the input for model explanation. SmoothGrad [26] aggregates input gradients across input samples with Gaussian noise, leading to a notable enhancement in localization ability. FullGrad [10] further integrates gradients from model biases, satisfying additional axioms. To guarantee completeness, integrated gradients (IG) [8] integrates gradients from a reference to the input. However, its performance depends on the choice of reference. To improve reference reliability, IG-SG [26], IG-SQ [18] and IG-Uniform [33] employ perturbed inputs as references. EG [13] employs training samples as references to maintain the distribution invariance. Pan et al. [34] calculated class-specific adversarial samples as the reference. Yang et al. [28] recalibrated attributions with valid references. Akhtar and Jalwana [35] improved IG attribution credibility with a better choice of reference and a modified integration process. Wang et al. [27] explained a contrastive output for distinctive attributions, leading to class-contrastive attributions.

2.2 XAI Benchmarks

Numerous model explanation methods have given rise to a multitude of XAI benchmarks. LeRF and MoRF [15] are extended from pixel flipping [14], which perturbs input samples to test output changes. Similarly, insertion and

deletion games [16] offer a benchmark for evaluating attributions of a single input sample. However, Hooker et al. [18] revealed that perturbed images cause input distribution shift, making the benchmarking unreliable. Therefore, ROAR [18] and DiffROAR [36] were proposed to retrain models on the perturbed images, ensuring models are learned within the distribution. ROAD [17] and DiffID [37] offer alternative methods to mitigate input distribution shift without necessitating costly model retraining. On the other hand, sensitivity-n [38], SENS_{MAX} and INFD [39] focus on testing the fidelity of attributions by perturbing the input. Adebayo et al. [40] randomized the model parameters and training labels to test the sanity of attributions. Other efforts have also been made to provide ground truth for the estimated attributions. DiFull, DiPart [20] and Pointing Game [19] employ training annotations for attribution evaluation. Khakzar et al. [41] used model-optimized features as proxy for attribution ground truth. Lin et al. [22] benchmarked explaining tools through analyzing the detection of visible triggers in input for Trojaned models. Additionally, Arras et al. [21] employed the controlled VQA framework to generate synthetic images for benchmarking.

2.3 Neural Backdoor

Backdoors alter a model’s predictions by making it sensitive to certain trigger patterns. This framework is relevant because we leverage backdoors in our BackX. Gu et al. [23] introduced BadNet which mislabels and stamps triggers to poison the training samples. Blended attack [24], ISSBA [25] and WaNet [42] are proposed to generate more stealthy sample-specific triggers, achieving invisible poisoning. Adap-Blend [43] further enhances the stealthiness of attack in the latent space. Due to the clear attribution of backdoor triggers in the models trained to achieve it, we leverage neural backdoors to circumvent the lack of ground truth in attribution evaluation. Given the wide applications of attribution methods in backdoor defense [12], [44], we provide guidance for defense against backdoor attacks using attributions as part of this study.

3 ON BENCHMARK FIDELITY

In this section, we first put forth a set of criteria that a reliable explanation benchmark should adhere to. We then compare existing benchmarks on the proposed criteria.

Let us consider an input sample $x \in \mathbb{R}^n$ with its label $y \in \mathbb{R}^c$ from a dataset \mathcal{D} . A classifier denoted as $f : \mathbb{R}^n \rightarrow \mathbb{R}^c$ is parameterized by θ . To explain the model’s prediction $f(x)$, an attribution explaining tool $\phi : \mathbb{R}^c \rightarrow \mathbb{R}^n$ is used to generate an attribution map M , specifically $M = \phi(f(x))$. An XAI benchmark intends to faithfully evaluate the reliability of the explanation M . For a quick reference, we also provide a summary of the notations used in the article in Appx. 9.

3.1 Fidelity Criteria

Our fidelity criteria are based on clear observations, hence they are generally intuitively understood. It is worth emphasizing that our intention of providing the criteria is not to establish exhaustive guarantees for benchmark reliability.

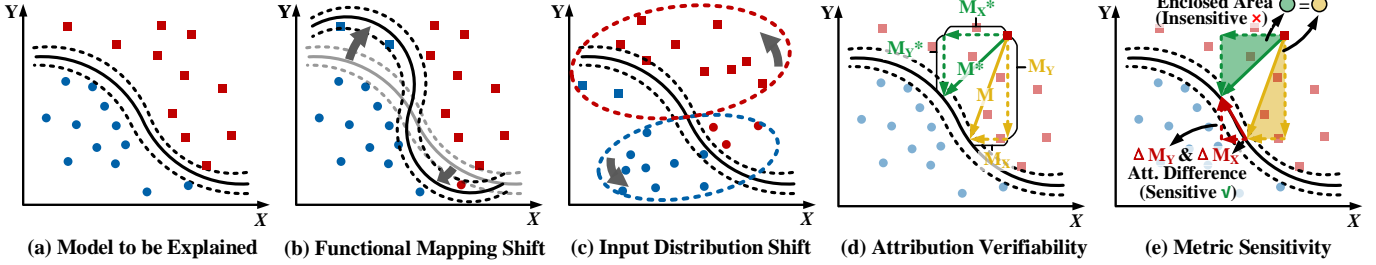


Fig. 1. Illustration of fidelity criteria. For explaining (a) the model, a faithful XAI benchmark should avoid (b) Functional Mapping Shift, and (c) Input Distribution Shift, while ensuring (d) Attribution Verifiability, and (e) Metric Sensitivity. See § 3.1 for explanations.

Due to the abstract nature of the notion of reliability, it is debatable if such a set of guarantees even exists. Here, we aim at identifying clear foundational properties that are intuitively verifiable through observations.

1) *Functional Mapping Invariance*: Given a model f to be explained, e.g., Fig. 1(a), functional mapping invariance requires that the attribution benchmarking process does not cause a functional mapping shift to the model, see Fig. 1(b). Suppose a perturbation ζ is imposed on the model f for benchmarking, resulting in $\zeta(f(x)) \neq f(x)$. The perturbation ζ can cause divergent explanations, making it challenging to ascertain whether the misalignment between the explanations and the model’s predictions stems from the unreliable explanatory tools or the functional mapping shift. Thus, functional mapping invariance is crucial for upholding the benchmark fidelity to the explained model.

2) *Input Distribution Invariance*: Input distribution invariance mandates the constancy of the input distribution $\mathcal{P}_{\mathcal{D}}$ in benchmarking. Assuming ξ represents an input perturbation that leads to input distribution shift (i.e., $\mathcal{P}_{\mathcal{D}} \neq \mathcal{P}_{\xi(\mathcal{D})}$). This shift causes explanation variation from the input samples to the perturbed input samples [18] - see Fig. 1(c). Similar to *functional mapping shift*, input distribution shift can also result in divergent explanations, obscuring the true cause of misalignment between the explanations and the model’s predictions. Thus, maintaining input distribution invariance is crucial for ensuring the benchmark’s fidelity to the explained samples.

3) *Attribution Verifiability*: This criterion requires that the correctness of the estimated attributions is verifiable. Given attributions $M = \phi(f(x))$, a faithful benchmark should be able to provide corresponding ground truth attributions M^* . The ground truth M^* is crucial for reliable benchmarking. Fig. 1(d) illustrates the idea where the normal vector from a sample to the decision boundary and its horizontal and vertical components provide the ground truth attributions ($M^* = M_X^* + M_Y^*$), allowing verification of an estimated attribution ($M = M_X + M_Y$) in a quantifiable manner.

4) *Metric Sensitivity*: Metric sensitivity requires that the metric used by the benchmark exhibits sensitivity to the attribution change. Fig. 1(e) shows examples of both sensitive and insensitive metrics. Given the estimated attribution M with its corresponding ground truth M^* , an insensitive metric, such as the area enclosed by the normal vectors and their components, yields identical results for both M^* and M . Thereby, failing to accurately quantify the differences

TABLE 1
Fidelity criterion fulfillment of XAI benchmarks.

Fidelity Criteria	Explainable AI Benchmarks									
	MoRF; LeRF; Sensitivity-n; ROAR; Ins.& Del. Game	Pointing Game; Model & label randomization; ROAR; DiffROAR	DiFull & DiPart	Null Feature; Neural Trojan	Our BackX Benchmark	CLEVR-XAI				
Funct. Mapping Inv.	●	○	●	●	○	●	●	●	●	●
Input Dist. Inv.	○	●	●	●	●	●	●	●	●	●
Attr. Verifiability	○	○	○	●	●	●	●	●	●	●
Metric Sensitivity	●	●	●	●	●	●	●	●	●	●
Desirability Score	2	2	2.5	3	2	2.5	2.5	3.0	3.5	

● = Strong (1); ● = Weak (0.5); ○ = No fulfillment (0).

between the attributions. In contrast, the difference between the estimated attribution M^* and the ground truth M ($\Delta M_X + \Delta M_Y$) serves as a sensitive metric, demonstrating a faithful sensitivity to the changes in the attributions.

3.2 Fidelity Comparison

In Tab. 1, we present a comparative analysis of different benchmarks with regard to their fidelity criteria assurance. Below, we discuss the details of the ratings provided in the table following three categories of the methods based on their underlying techniques.

1) *Input Perturbation-based Methods*. Since attribution maps are expected to highlight important input features, attribution benchmarks, including MoRF, LeRF [15], Ins.&Del. Games [16], DiffID [37] and ROAD [17], assess attribution methods by iteratively replacing pixels with zero or noise pixels. However, the input change causes an input distribution shift [18], compromising the reliability of evaluation outcomes. To ensure *input distribution invariance*, ROAR [18] and DiffROAR [36] retrain the model using perturbed input samples to incorporate the perturbed input samples within the training distribution. However, retraining models violate the criterion of *functional mapping invariance*. Thus, input perturbation-based attribution benchmarks shown in columns 1-3 of Tab. 1 struggle to ensure invariance to input distribution and the explained model.

2) *Sanity and Sensitivity Checks*. Sanity and sensitivity checks are originally proposed to test the fidelity of attri-

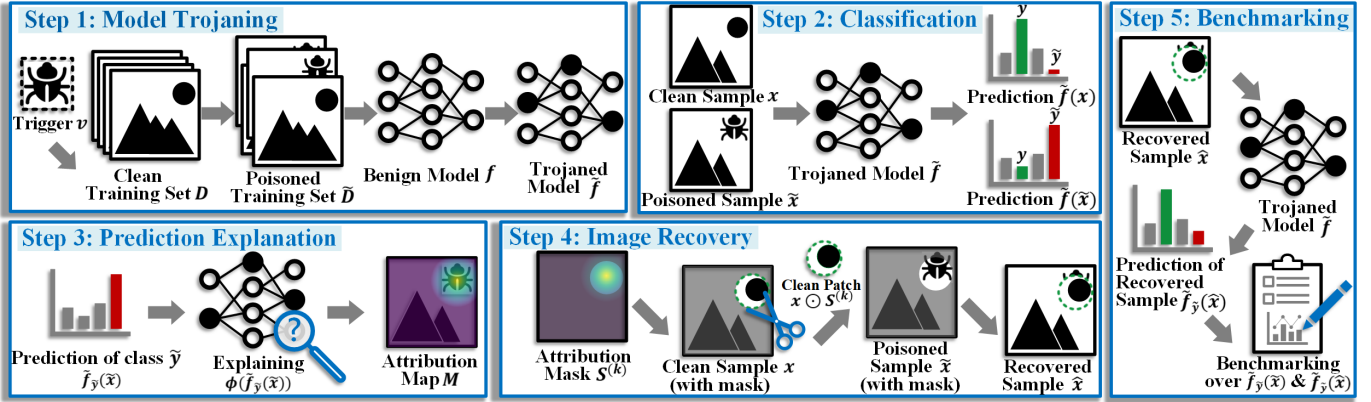


Fig. 2. The pipeline of BackX. **Step 1** embeds a backdoor into a benign model by retraining it on a poisoned training set. **Step 2** uses the Trojaned model to generate predictions. **Step 3** applies attribution methods to explain the predictions. **Step 4** recovers a sample from poisoned sample by replacing its pixels from clean sample, as guided by attribution mask. **Step 5** assesses attribution methods.

bution methods for the explained input samples and models. Benchmarks such as sensitivity-n [38], SENS_{MAX} , and INF D [39] aim to assess the sensitivity of attribution methods under input perturbations. While these benchmarks provide valuable assessment targets, these targets are unachievable by attribution methods in practice, resulting only in a partial guarantee of *attribution verifiability*. Adebayo et al. [40] randomized model parameters and training labels to test the sanity of attributions. However, this sanity check can lead to a functional mapping shift. Similar to the input perturbation-based techniques, sanity and sensitivity checks in columns 4-5 of Tab. 1 rely on input or model perturbations, making it challenging to simultaneously satisfy both *input distribution invariance* and *functional mapping invariance*.

3) *Benchmark with Attribution Ground Truth*. Other attribution benchmarks have made efforts to establish attribution ground truth for assessing attribution methods. Pointing Game [19], DiFull & DiPart [20] utilize training annotations as attribution ground truth. However, training annotations only offer partial ground truth information for attributions. Khakzar et al. [41] calculated Null Feature without class information through model optimization as the ground truth for attributions. However, there remains a notable absence of evidence substantiating the relationship between the features generated by model optimization and their corresponding attributions. CLEVR-XAI [21] employs a visual question-answering framework to generate synthetic images to provide controlled evaluations of generated objects. However, the presence of shadows from these objects compromises the strict confinement of attribution to the objects’ physical areas. Lin et al. [22] employ neural Trojan for providing attribution ground truth, but their benchmark fails to guarantee that the model prediction change is solely attributable to Trojaned features. In addition to the partial guarantee of *attribution verifiability*, these attribution benchmarks evaluate the ratio between the defined ground truth region and the region with high attributions, compromising sensitivity in their evaluation metrics for attributions. From Tab. 1, it is evident that a full guarantee of attribution verifiability presents a significant challenge.

Overall, our benchmark, discussed in the forthcoming section, stands out as more desirable than the existing

techniques on the fidelity criteria.

4 BACKX BENCHMARK

In this section, we commence by illustrating the pipeline of our BackX benchmark and then we introduce a set of metrics carefully crafted to evaluate the capabilities of attribution methods. Finally, we provide a discussion on the assurance of benchmark fidelity criteria in the BackX benchmark.

4.1 Benchmark Framework

In Fig. 2, we present an illustration of our BackX benchmark pipeline. Given a clean training set \mathcal{D} , we generate a poisoned training set $\tilde{\mathcal{D}}$ by incorporating a trigger v into certain portions of the clean samples and modifying the true label y with the poisoned target label \tilde{y} . This poisoned training set is then used to transform a benign model f into a Trojaned model \tilde{f} in Step 1 of Fig. 2. The Trojaned model is employed to generate predictions $\tilde{f}(x)$ and $\tilde{f}(\tilde{x})$ of clean and poisoned samples x and \tilde{x} , as shown in Step 2 of Fig. 2. Then, an attribution method ϕ explains the output prediction $\tilde{f}_{\tilde{y}}(\tilde{x})$ for class \tilde{y} , producing an attribution map M - Step 3 of Fig. 2. Subsequently, a mask $S^{(k)} \in \{0, 1\}^n$ is computed, identifying the top $k\%$ most important input features (e.g., input pixels) as specified by the attribution map. The mask is then utilized to remove the poisoned portion of the sample to construct a recovered sample \hat{x} , see Step 4 of Fig. 2. Specifically, a clean patch is extracted from the clean image using the mask. The recovered sample is constructed by replacing the corresponding pixels in the poisoned sample with the extracted patch. Mathematically, the recovered sample \hat{x} is defined as

$$\hat{x} = \tilde{x} \odot (\mathbf{1} - S^{(k)}) + x \odot S^{(k)}. \quad (1)$$

Here, the recovered sample \hat{x} estimated from a faithful attribution method is expected to be an accurate transformation of the poisoned sample \tilde{x} to its clean counterpart x . Thus, attributions $\phi(\tilde{f}(x))$ for the predictions on the clean samples serve as the attribution ground truth for the recovered sample. Driven by the attainability of ground truth, we benchmark attribution methods using the backdoored model, as illustrated in Step 5 of Fig. 2.

In BackX, we comprehensively incorporate both visible and invisible trigger patterns for backdoored models through Blend [24] and ISSBA [25] techniques. For the complete control, we enhance the Blend attack with a watermark trigger to ensure poisoned samples align with the original distribution, focusing the backdoored model solely on the trigger region. The watermark trigger is created using the formula

$$v^{(\alpha)} = \alpha \cdot v + (1 - \alpha) \cdot x \odot S^*, \quad (2)$$

where $\alpha \in [0, 1]$ represents the visibility of the trigger, and $S^* \in \{0, 1\}^n$ is the mask of trigger v . ISSBA attack is utilized to generate input-specific invisible triggers. Further details on the backdoored models and triggers used in our experiments are presented in Appx. 11.

4.2 Evaluation Metrics

In this section, we define a set of metrics specifically tailored to our backdoor-based evaluation for the BackX benchmark.

1) *Attack Success Rate*: Attack Success Rate (ASR) is a prevalent metric in backdoor attacks [45], [46]. It records the success of target prediction label \tilde{y} for the input samples with true label y when the trigger is embedded in the input samples. In our context, the ASR is formally defined as

$$\text{ASR} = \mathbb{E}_{(x,y) \sim \mathcal{D}} \mathbf{I}[\hat{y} = \tilde{y} | y \neq \tilde{y}], \quad \hat{y} = \arg \max_i \tilde{f}_i(\hat{x}). \quad (3)$$

Here, the ASR is computed as an expectation over samples drawn from a dataset \mathcal{D} through a boolean function $\mathbf{I}[\cdot]$. In our benchmark, we leverage ASR to evaluate the ability of attribution methods to successfully identify the trigger with the recovered sample \hat{x} .

2) *Trigger Recall*: In addition to evaluating predictive performance, we assess the localization capability of attribution methods. Trigger Recall (TR) is introduced to evaluate the ability of an attribution method to locate the embedded triggers. TR computes an expectation over poisoned samples \tilde{x} by evaluating the alignment between its trigger mask $S_{\tilde{x}}^*$ and the attribution mask $S_{\tilde{x}, \tilde{y}}^{(k)}$ of target class \tilde{y} as

$$\text{TR} = \mathbb{E}_{(x,y) \sim \mathcal{D}} S_{\tilde{x}, \tilde{y}}^{(k)} \cap S_{\tilde{x}}^* / S_{\tilde{x}}^*, \quad y \neq \tilde{y}, \quad (4)$$

where $S_{\tilde{x}, \tilde{y}}^{(k)}, S_{\tilde{x}}^* \in \{0, 1\}^n$, and $k \in [0, 1]$ denotes the fraction of the most important features identified by the attribution method in the input. It is worth noting that the recall rate of the detected trigger equates to *precision* when the recovery rate k equals the proportion of the trigger in the input.

3) *Logit and Probability Fractional Change*: To evaluate the detailed prediction change, we measure the logit fractional change of target class \tilde{y} as $\Delta f_{\tilde{y}}(\hat{x})$. In our context, this measure quantifies the extent to which the attribution method can help reduce the confidence of the target class \tilde{y} when recovery is made by replacing the features identified as trigger features by attributions. We similarly denote the logit fractional change of the output for the true label y as $\Delta f_y(\hat{x})$. This serves to quantify the extent to which the attribution method can help restore the confidence in the class y . Concretely, the logit and probability fractional changes through the backdoored model \tilde{f} are defined as

$$\Delta \tilde{f}_{\tilde{y}}(\hat{x}) = \frac{\tilde{f}_{\tilde{y}}(\hat{x}) - \tilde{f}_{\tilde{y}}(x)}{\tilde{f}_{\tilde{y}}(\hat{x}) - \tilde{f}_{\tilde{y}}(x)}, \quad \Delta \tilde{f}_y(\hat{x}) = \frac{\tilde{f}_y(\hat{x}) - \tilde{f}_y(\tilde{x})}{\tilde{f}_y(x) - \tilde{f}_y(\tilde{x})}. \quad (5)$$

To direct the metric's focus solely on the attribution of introduced trigger features, we further subtract $\tilde{f}_{\tilde{y}}(x)$ and $\tilde{f}_y(\tilde{x})$ from predictions on \hat{x} and their corresponding reference predictions $\tilde{f}_{\tilde{y}}(\tilde{x})$ and $\tilde{f}_y(x)$ to eliminate the potential class information from x and \tilde{x} . Let $p(x) = \text{softmax}(\tilde{f}(x))$ denote the probability output through a softmax function. The fractional change of output probabilities $\Delta p_{\tilde{y}}(\hat{x})$ and $\Delta p_y(\hat{x})$ can be similarly defined to measure changes of normalized outputs in class \tilde{y} and y . We avoid their formulas for conciseness. Here, we further combine these two metrics to simultaneously assess two critical aspects: the ability to restore predictive confidence in the clean class and the capability to reduce the confidence score of the poisoned class. Taking the fractional logit change (FLC) as an example, we combine two metrics as

$$\text{FLC} = \mathbb{E}_{(x,y) \sim \mathcal{D}} \|\Delta \tilde{f}_y(\hat{x})\|^2 + \|1 - \Delta \tilde{f}_{\tilde{y}}(\hat{x})\|^2, \quad y \neq \tilde{y}. \quad (6)$$

This test also serves to guard against attributions being influenced by adversarial perturbations. For instance, if an attribution method is derived from the adversarial attack, it may significantly decrease the confidence score of the poisoned class but fail to restore the predictive confidence of the clean class. Such methods cannot be regarded as reliable but result in an overly positive assessment of adversarial-based attribution methods. Thus, we rigorously assess attribution methods based on their performance in both recovery and suppression capabilities.

4.3 Benchmark Fidelity Examination

In this part, we closely examine the crucial aspect of BackX regarding satisfying the fidelity criteria set out in Sec. 3.1. In what follows, we delve deeper into theoretical details only when a criterion fulfillment is not obvious.

1) *Functional Mapping Invariance & Metric Sensitivity*: By consistently employing the same backdoored model \tilde{f} throughout the benchmarking process, the BackX framework intrinsically ensures *Functional Mapping Invariance*. Additionally, the introduced three metrics are capable of benchmarking attributions at *element* level. This ensures the preservation of *Metric Sensitivity*.

2) *Input Distribution Invariance*: In BackX, we evaluate the attribution methods via backdoored models. Assume a benign model f is trained to classify an input sample x into a label y , constrained within a boundary ϵ measured by a metric Ω . Here, the model's prediction remains consistent despite the perturbation δ , such that $f(x + \delta) = y$, under the constraint $\Omega(x, x + \delta) \leq \epsilon$. Consider a poisoned sample $\tilde{x} = x + v$, where \tilde{x} is constrained by $\tilde{\epsilon}$, i.e., $\Omega(\tilde{x}, x) \leq \tilde{\epsilon}$. A backdoor manipulates the boundary $\tilde{\epsilon}$ to yield a poisoned model \tilde{f} , thus resulting in misclassification of the poisoned sample \tilde{x} into a target class \tilde{y} . The recovered sample \hat{x} is derived to convert the poisoned sample \tilde{x} back to the clean state x . The transformation on \hat{x} is bounded by \tilde{x} and x , i.e., $\Omega(x, \hat{x}) \leq \Omega(x, \tilde{x})$. If $\tilde{\epsilon} \leq \epsilon$, meaning the modified perturbation boundary $\tilde{\epsilon}$ is smaller than or equal to the original boundary ϵ , then the recovered sample \hat{x} is preserved within the original training distribution. We summarize this relationship as the following proposition.

Proposition 1. *A benign model f classifies inputs x with perturbation δ to labels y within a boundary ϵ defined by metric Ω , with $f(x + \delta) = y$ under $\Omega(x, x + \delta) \leq \epsilon$. Assume $\tilde{x} = x + v$ constrained by $\tilde{\epsilon}$ backdoors f to misclassify \tilde{x} to target \tilde{y} . Recovering \hat{x} from \tilde{x} to x constrained by $\Omega(x, \hat{x}) \leq \Omega(x, \tilde{x})$ preserves \hat{x} within the original training distribution if $\tilde{\epsilon} \leq \epsilon$.*

The proof of the proposition is provided in Appx. 10. Given the stealthy nature of neuron backdoors, the constraint of $\tilde{\epsilon}$ is negligibly small for well-trained models [47], which implies $\Omega(x, \hat{x}) \leq \Omega(x, x + \delta)$. This suggests that $\tilde{\epsilon} \leq \epsilon$, thereby largely preserving the benchmarked samples within the original distribution. Whereas we acknowledge that BackX cannot perfectly eliminate the influence of input distribution shift [18], the *Input Distribution Invariance* is only subtly disturbed, bounded by ϵ . It is noteworthy that our trigger recall metric offers a guarantee of *Input Distribution Invariance* at the expense of sacrificing the guarantee of *Metric Sensitivity*.

3) *Attribution Verifiability (Model backdoor and Metrics):* To guarantee attribution verifiability, we carefully devise techniques for both backdoor and metric design to ensure that the prediction changes are fully attributed to the trigger features. During backdooring the model, we maintain low loss for both poisoned and clean samples while ensuring that trigger features substantially alter the prediction accuracy on poisoned samples, achieving up to 100% success, as shown in Tabs 3-5 of Appx. E. The employed watermark trigger also overlapped with different input features, serving as data augmentation, facilitating the predictive performance change to be exclusively attributed to the introduced trigger features.

Although the exclusivity of the trigger in the backdoored model helps the fidelity of the proposed metrics, logit and probability fractional change require a further careful design to ensure correct attribution ground truth. Consider the logit fractional change metric $\Delta \tilde{f}_y(\hat{x})$ defined in Eq. 5 that examines the extent to which the logit of the recovered sample \hat{x} can be restored from a poisoned sample \tilde{x} for the clean class y . It should be noted that the poisoned sample always contains class information corresponding to the class y . Consequently, directly computing the fractional change in output logits, i.e., $\tilde{f}_y(\hat{x})/\tilde{f}_y(x)$, may compromise the reliability of benchmarking results, given the intrinsic information of y . To address this concern, we eliminate this potential class information by subtracting the predictive confidence $\tilde{f}_y(\tilde{x})$ on samples of the class y from the metrics, thus ensuring a reliable assessment.

4) *Attribution Verifiability (Feature Leakage):* Ensuring *Metric Sensitivity* implies that the primary focus of our benchmarking is placed on the recovered samples. These samples inadvertently hold information about the attribution mask used for image recovery - see Step 4 in Fig. 2. This can lead to unreliable benchmarking due to potential class information leakage through the mask [17], thereby compromising the fidelity of the provided attribution ground truth. Therefore, it is essential to rigorously check the leaked information of the recovery samples for the assurance of *Attribution Verifiability*.

We commence by examining the entropy of a singular

variable x , quantifying the amount of information as

$$H(x) = - \sum_{x_i \in x} P(x_i) \log P(x_i). \quad (7)$$

The classification performance is correlated with the mutual information $I(x; c)$ between the input x and a class c [48]. Without loss of generality, we can assume that attribution methods benchmarked using a masked sample \hat{x} quantify the mutual information $I(\hat{x}; c)$. Assuming the attribution mask S operates as a patch that directly removes features from the input sample, this process inevitably allows the leakage of class-related information into the masked sample \hat{x} , leading to a leakage of $I(S; c)$. The leakage leads to the unfaithfulness of evaluation results by introducing class information from S in \hat{x} , i.e., $I(\hat{x}; c) \neq I(c; \hat{x}|S)$. To ensure benchmarking fidelity, the leaked features from S should be eliminated, i.e., $I(S; c) \approx 0$. This relation is formalized by the below proposition.

Proposition 2. *By minimizing the mutual information $I(S; c)$ between the mask S and a class c , the leaked information from the attribution mask S to the masked sample \hat{x} can be alleviated, resulting in enhanced fidelity of the evaluation results, following $I(c; \hat{x}) \approx I(c; \hat{x}|S)$.*

The proof of the proposition is provided in Appx. 10. In contrast to the prevalent existing benchmarks that assess attributions through feature removal, our benchmark recovers the features of the poisoned sample with those of the clean sample through the mask, i.e., $S \odot x \in x$. The recovered features which are part of the clean sample x do not contain additional information related to the target class \tilde{y} . As a result, the leaked information from S to class \tilde{y} is negligible, if any. Thus, the evaluation process within our benchmark provides assurance of *Attribution Verifiability*. This also highlights an intrinsic superiority of our benchmark over the perturbation-based methods that are inadvertently influenced by feature leakage.

Overall, our benchmark offers the desired level of assurance for fulfilling the essential fidelity criteria, which is not achieved by the previous benchmarking techniques.

5 CONSISTENT ATTRIBUTION EVALUATION

Having established the foundations of a reliable benchmark for attribution methods, we further analyze the existing attribution techniques for their transparent benchmarking. Currently, a diverse range of attribution methods is available in the literature. It has been demonstrated that their evaluation results are significantly influenced by two common confounding factors, (1) post-processing techniques of attributions [26], [28] and (2) explained model outputs in attribution estimation [27]. However, to the best of our knowledge, no existing contribution explores a consistent evaluation paradigm for the different attribution methods. This section is aimed at establishing a fair paradigm for consistent benchmarking. To achieve that, we first discuss the attribution methods evaluated in this work, and their categories. Subsequently, our analysis is grounded in extensive experiments across diverse setups to establish a consistent setup¹.

1. Details of the models used in our experiments, as well as their comparisons, are reported in Appx. 11.2 and Appx. 12.

5.1 Attribution Methods and Categories

In our experiments, nine attribution methods are benchmarked including GCAM [32], FullGrad [10], Grad [6], GGCAM [32], SG [26], IG [8], IG-Uniform [33], AGI [34], and LPI [37]. We categorize these methods into three groups; namely *CAM-based*, *gradient-based*, and *integration-based methods*, based on their distinct underlying explanation processes, as explained below.

1) *CAM-based Methods*: Zhou et al. [31] proposed a class activation mapping (CAM) technique to localize the class-specific features of input samples. Assuming a feature map A^k of the k -th convolutional layer before a softmax layer, CAM-based attribution methods M_{CAM}^c (e.g., GCAM) calculate a weighted combination of activation maps A^k for a class c as

$$M_{CAM}^c(x) = \Psi(\text{ReLU}(\sum_k w_k^c A^k)), \quad (8)$$

where $w_k^c = \text{avg}(\sum_i \sum_j \partial f_c(x) / \partial A_{i,j}^k)$ indicates the activation weight by applying a global average pooling on the activation map A^k , and Ψ indicates an interpolation operator to estimate an attribution map with the same scale as x from a down-sampled activation map. In our experiments, we test two CAM-based attribution methods including GCAM and FullGrad. In contrast to CAM, GCAM avoid the use of additional structures enabling a generalized applications. FullGrad further integrates gradients of model biases to ensure the completeness axiom [8]. Since FullGrad retains a similar process of utilizing an interpolated activation map, we categorize it alongside GCAM as a CAM-based method. Although other CAM-based attribution methods also exist [49], [50], we test two representative ones in our experiments to cover this category.

2) *Gradient-based Methods*: Gradient-based attribution methods, such as Grad [6], employ a first-order Taylor expansion to approximate the non-linear model: $f_c(x) \approx w^T * x + b$. Thus, the attribution of an input sample x for a class c , can be computed using the gradients with respect to the input as

$$M_{\text{Grad.}}^c(x) = \partial f_c(x) / \partial x. \quad (9)$$

In contrast with CAM-based attribution methods, gradient-based methods are capable of estimating attribution values at the element level for each input feature, eliminating the need for interpolation operators. In our experiment, we categorize GGCAM alongside Grad and SG as gradient-based attribution methods. The GGCAM leverages Grad to guide GCAM in performing element-wise attribution estimation.

3) *Integration-based Methods*: Compared to gradient-based attribution methods, integration-based attribution methods integrate input gradients from a reference input x' to the feature x along an integral path. Taking IG as an example, the attribution of an input feature x_i for a class c can be estimated as

$$M_i^c \text{ Integr.}(x, x') = (x_i - x'_i) \times \int_{\alpha=0}^1 \frac{\partial f_c(\tilde{x})}{\partial \tilde{x}_i} \Big|_{\tilde{x}=x'+\alpha(x-x')} d\alpha, \quad (10)$$

where α indicates a linear integration path from the reference input x' to the input x , and x' is typically set as a zero vector in IG. Different integration-based attribution

methods (IG-Uni, IG-SG [26], AGI, and LPI) are proposed to redefine the reference and the integral path. As these methods share the approach of estimating integrals to offer explanations, we categorize these methods as integration-based attribution methods. Due to their distinct theoretical guarantees in using different references [8], [37], we benchmark four integration-based attribution methods including IG, IG-Uni, AGI and LPI.

4) *Other Methods*: A variety of attribution methods also have been proposed for providing explanations through feature perturbation or removal (e.g., LIME [51], SHAP [52], occlusion [7], and mask [53]). However, these perturbation-based methods are revealed to exhibit unreliabilities [8], [9], as well as entailing a significant computational cost [38]. Therefore, we exclusively evaluate the propagation-based attribution methods. On the other hand, a few attribution methods, e.g., LRP [54] and DeepLift [9], fail to satisfy basic axioms like *completeness* and *implementation invariance*. Hence, these methods are not included in our evaluation.

Overall, we benchmark two *CAM-based* methods (GCAM and FullGrad), three *gradient-based* methods (Grad, GGCAM and SG), and four *integration-based* methods (IG, IG-Uni, AGI and LPI).

5.2 Post-processing Choice

It is currently prevalent to use any of the absolute or original attribution scores (as computed by an attribution method) to explain model predictions, despite the fact that these two choices yield distinct explanations. In Figure 3, we provide visualizations of employing absolute and original attributions for different methods. There is a notable disparity in the highlighted regions of input samples between the two post-processing techniques. This underscores the susceptibility of visual outcomes to ambiguity, emphasizing the necessity of quantitative assessments to provide clarity and

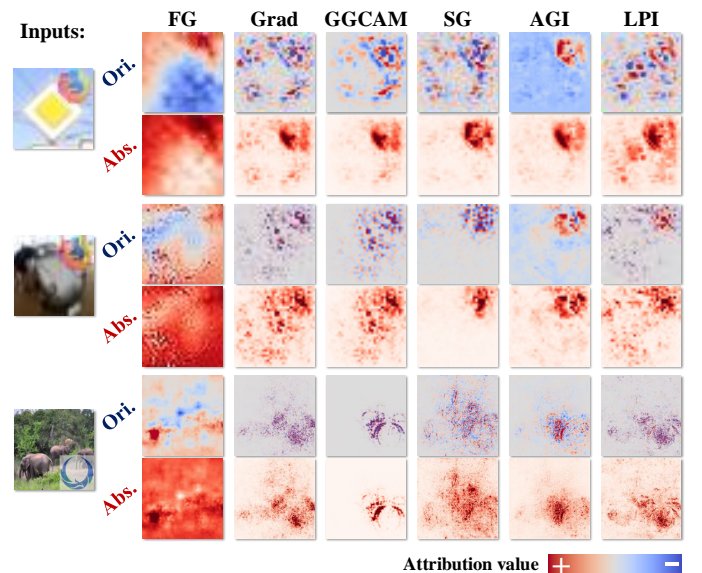


Fig. 3. Visualization of absolute and original attributions for input samples from GTSRB, CIFAR-10 and ImageNet respectively. The predictions made by models backdoored through Blend attack with trigger visibility of 0.5 are explained using attribution methods.

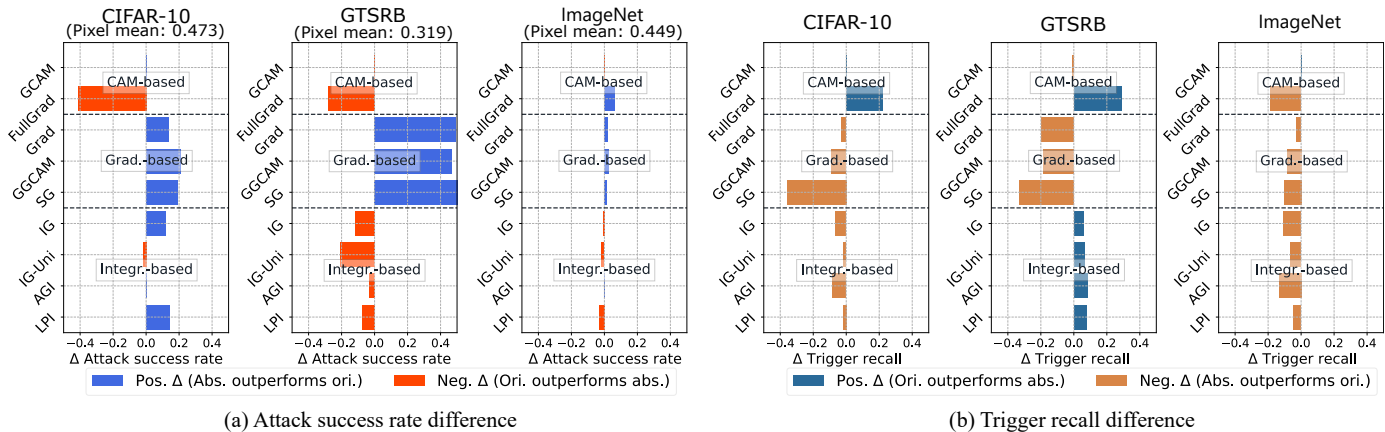


Fig. 4. The performance comparison of CAM-based, gradient-based and integrated-based attribution methods on CIFAR-10, GTSRB and ImageNet using BackX benchmark. **(a)** Difference in Attack Success Rate between benchmarking absolute values (abs.) and original values (org.) of attributions is calculated. **(b)** Trigger Recall difference with and without taking absolute values.

context. This problem is more pronounced for smaller input images due to the limited number of pixels. Although large ImageNet size images may yield more consistent attribution maps, it is crucial to recognize that their relative feature importances undergo shifts, often reflected in attributions alternating between negative and positive values. This begs for an enquiry into the right choice between the original and absolute values for benchmarking.

In Fig. 4, we analyze the attack success rate and trigger recall for the two post-processing choices under BackX while fixing the image recovery equal to the trigger ratio. To facilitate comparison, we calculate the differences in benchmarking results between absolute and original values of attributions. The analysis is performed for CIFAR-10 [55], GTSRB [56] and ImageNet [57] datasets. For CAM-based methods, it can be observed that GCAM maintains consistent results across the datasets and our metrics². FullGrad’s integration of gradients from biases leads to fluctuations among the datasets. In contrast, all three gradient-based methods consistently rely on taking absolute attribution values across all the datasets for improved performance. The results align with the finding of Smilkov et al. [26], suggesting that taking the absolute value of gradients can produce clearer attribution maps. One plausible explanation behind the insensitivity of gradient-based methods to the sign of attributions lies in their focus on capturing the magnitude of each feature’s influence on the model output using input gradients, irrespective of the direction of change in the feature’s value.

On the other hand, integration-based methods have a slightly more stable performance for different datasets. Their reliance on absolute values of attributions decreases as the mean value of the image pixels decreases. This can be attributed to the fact that these techniques accumulate gradients from a reference input. Images with lower mean pixel values tend to reduce the undesired gradient fluctuations due to their natural proximity to the reference. We draw the following observation from our analysis.

2. While ReLU is typically applied to CAM-based results, we intentionally remove ReLU to preserve the original attributions.

Observation 1

Basic CAM-based methods remain largely insensitive to post-processing techniques. Gradient-based attribution methods consistently depend on computing absolute attributions, whereas this reliance decreases in integration-based methods with a reduction in the mean pixel value.

Based on our observation, we choose the absolute attributions for gradient-based methods in the subsequent experiments. CAM-based and integration-based methods employ the original attributions to ensure the satisfaction of their well-known axioms³.

5.3 Output Choice

In general, contemporary attribution methods lack a clear distinction between using model logits and softmax probabilities as the model output for computing the attributions [27]. This can compromise benchmarking transparency. In Fig. 5, we compare the attack success rate and trigger recall on BackX benchmark when attributions use output logits and probabilities on CIFAR-10, GTSRB, and ImageNet. Following the conventions from Fig. 4, we report the differences between the values.

The results demonstrate that CAM-based methods tend to rely on explaining probabilities to achieve better performance, whereas integration-based methods prefer explaining output logits. Gradient-based methods exhibit a significant fluctuation between explaining logits and probabilities. Moreover, explaining logits leads to stronger localization capabilities in both gradient-based and integration-based attribution methods, as implied by the results in Fig. 5(b). This is indicative of the inherent richness of raw logits in facilitating class localization.

It is worth noting that the attribution differences between the choices of logits and probabilities become narrower as the number of classes increases. This convergence is attributed to softmax normalization, which redistributes probability mass more evenly across categories. This phenomenon is mathematically evident in the softmax function,

3. FullGrad and integration-based methods are able to satisfy the completeness axiom with their original attributions.

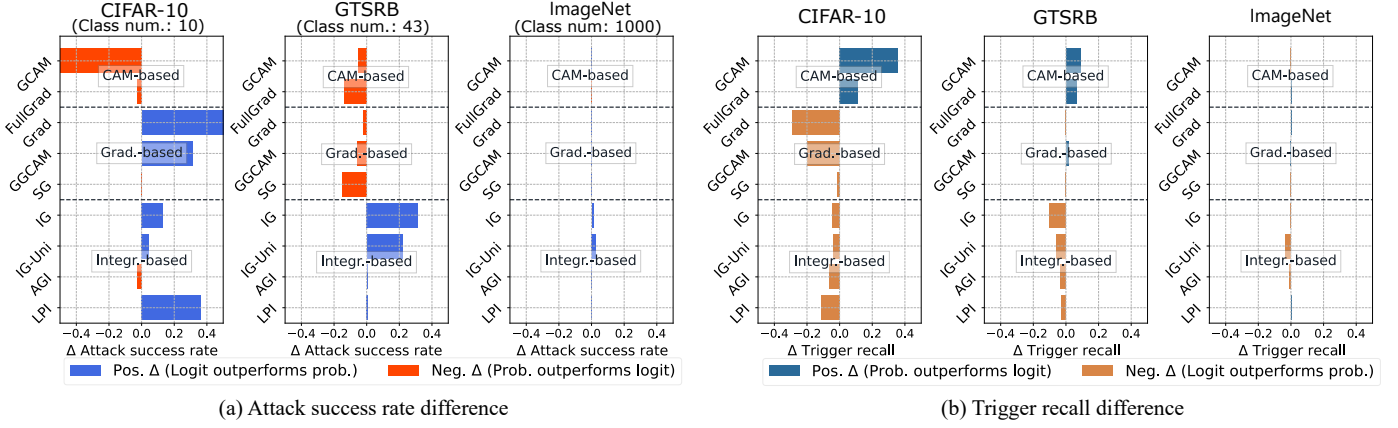


Fig. 5. The performance comparison of CAM-based, gradient-based and integrated-based attribution methods for output choice. **(a)** Difference between attack success rate when attributions are computed for softmax probabilities (prob.) and logits. **(b)** Trigger recall difference using softmax probabilities and logits.

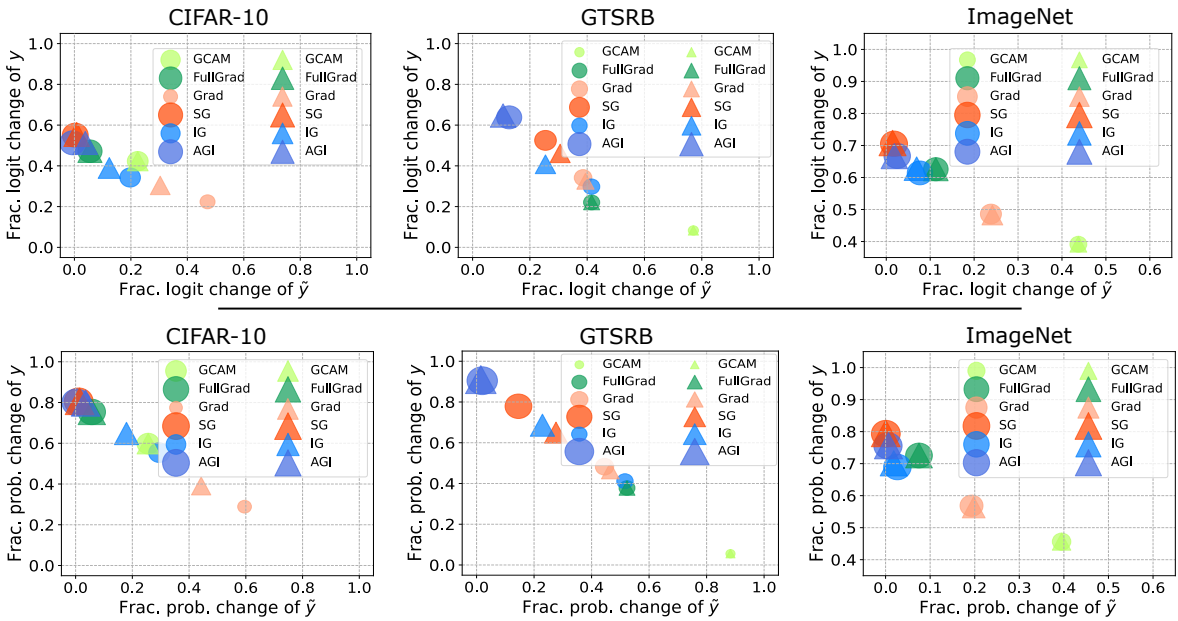


Fig. 6. Comparison of fractional logit change (**top row**) and fractional probability change (**bottom row**) between explaining logits and probabilities. Approaching top-left corner in each plot indicates superior performance. ● denotes that probabilities are explained with attribution methods. ▲ indicates that logits are explained with the attribution methods.

where the denominator $\sum_{j=1}^N e^{z_j}$ increases with the total number of categories N , leading to the convergence of probabilities.

In Fig. 6, we show the comparison of fractional logit and fractional probability change between the attributions across three datasets. This evaluation combines fractional change of both y and \tilde{y} to compare the capability of attribution methods in reducing output of \tilde{y} and recovering output of y . All methods are scaled by their distance to the bottom left corner as defined in Eq. 6. Methods are represented by markers of a circle (●) and a triangle (▲) to separate attributions estimated in explaining output probabilities and logits. The evaluation allows us to assess whether the results of attribution methods change when the evaluation target is altered. It is observed that the performance of various attribution methods remains consistent when evaluating fractional change in output probabilities and logits within

a specific dataset. This underscores the consistency in the preferences of attribution methods across different levels of predictive confidence, regardless of the specific objective being explained. These findings indicate the crucial role of establishing a clear and well-defined explanation setup in attribution methods. We make the following observation from the experiments.

Observation 2

CAM-based methods rely on output probabilities to gather distinctive class information to construct accurate activation maps. In contrast to output probabilities, explaining logits enables attributions to preserve unnormalized original activations for a class, leading to enhanced localization capability. However, the disparity of attributions between explaining logits and probabilities ultimately diminishes as the number of classes increases.

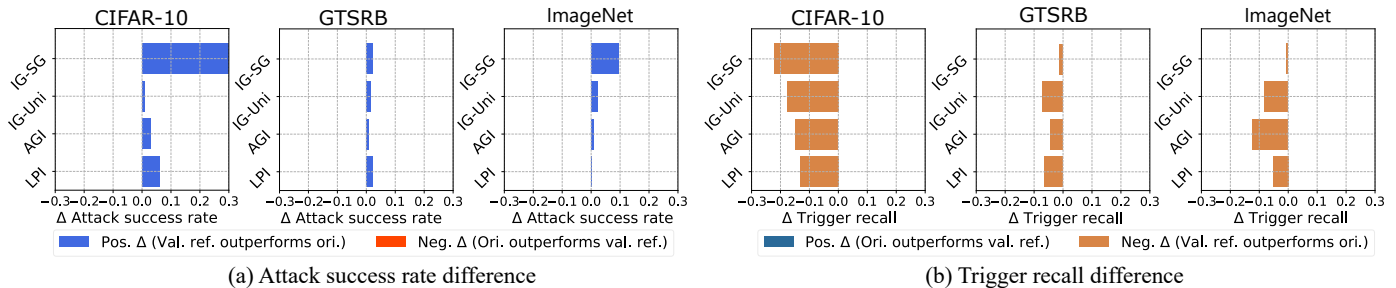


Fig. 7. The comparison of (a) attack success rate difference and (b) trigger recall difference between original attributions and attributions recalibrated by valid references. Four integration-based attribution methods are compared to explain the model’s output logit.

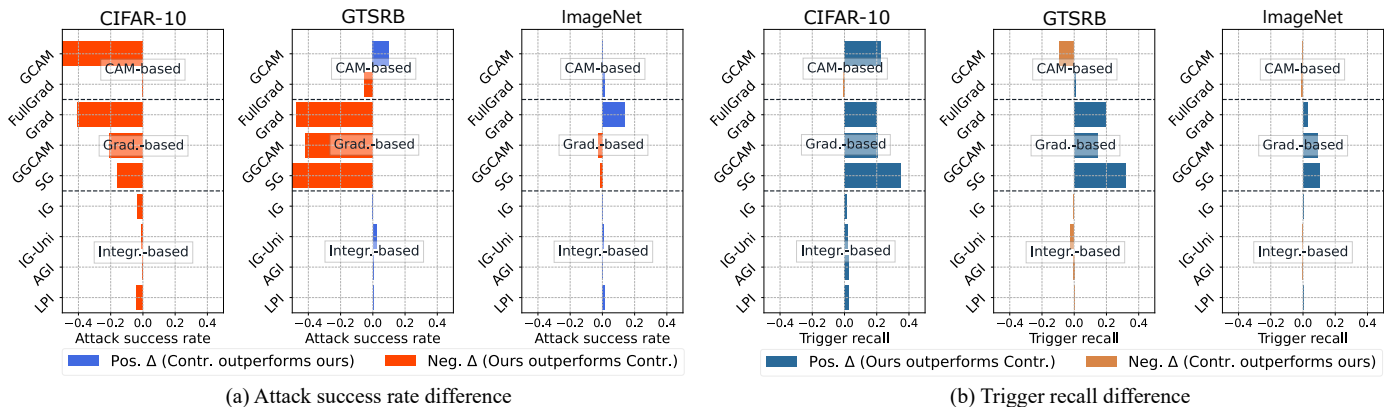


Fig. 8. The comparison of (a) attack success rate difference and (b) trigger recall difference between attributions estimated from our established consistent setup and attributions calculated by explaining the contrastive output.

Guided by this observation, we use CAM-based methods to explain output probabilities, while we use both gradient-based and integration-based attribution methods to explain logits in our subsequent experiments.

5.4 Re-Calibrating and Contrastive Output

Recent research has explored alternatives to enhance reliability of baseline attribution results [27], [28]. Here, we conduct comparative experiments for such choices. Re-calibrated attributions [27] have been introduced to enhance integration-based methods by estimating attributions from identified valid references. In Fig. 7, we compare the re-calibrated attributions and original attributions across integration-based attribution methods, including IG-SG, IG-Uni, AGI and LPI. It is observed that re-calibrated attributions further enhance the performance of the original attributions on CIFAR-10, GTSRB and ImageNet datasets. In addition, the performance of re-calibrated attributions is observed to degrade with decreasing mean input pixel values, aligning with our Observation 2. This demonstrates the sensitivity of integration-based methods to variations in the reference values. Despite the enhancement achieved through re-calibration, it remains unique to integration-based attribution methods. To maintain evaluation consistency across different methods, we retain the use of original attributions in the integration methods for the subsequent experiments.

Figure 8 offers a comparison between attributions computed by our established consistent setup and contrastive outputs [27] on CIFAR-10, GTSRB, and ImageNet. It is

notable that explaining contrastive output yields similar performance compared to explaining manually selected outputs, particularly evident in cases involving FullGrad and integration-based methods. This observation underscores the superiority of contrastive output over mutual selection. However, explaining contrastive output in CAM and Gradient-based methods does not achieve comparable performance. The following observation is derived from the above analysis.

Observation 3

The re-calibration technique consistently improves the performance of integration-based attribution methods. Attribution derived from explaining contrastive model output can achieve competitive results, particularly for CAM-based and integration-based methods.

In summary, our experimental results demonstrate that different setups yield distinctive performances for the same attribution method. This implies that the performance of these methods is susceptible to misinterpretation. We offer clear guidelines for consistent and fair benchmarking for the considered methods. To the best of our knowledge, there has been no prior research addressing the need for a standardized consistent setup. We advocate for the adoption of a unified configuration, which is imperative for the advancement of attribution methods.

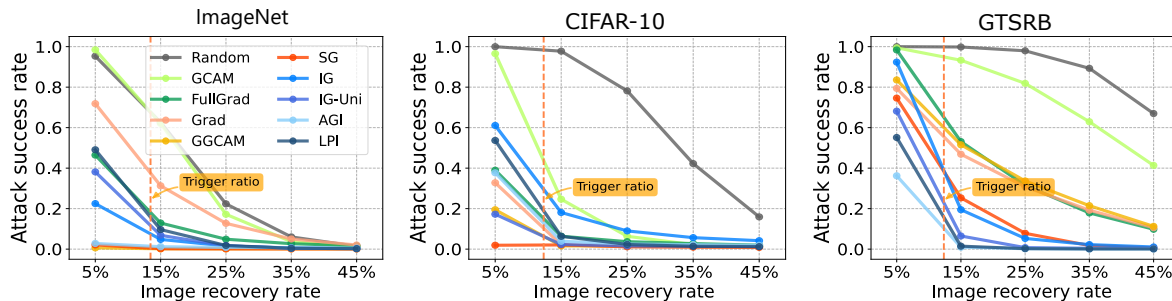


Fig. 9. Benchmarking of attribution methods under Blend attack using the attack success rate metric. Lower curves indicate better results.

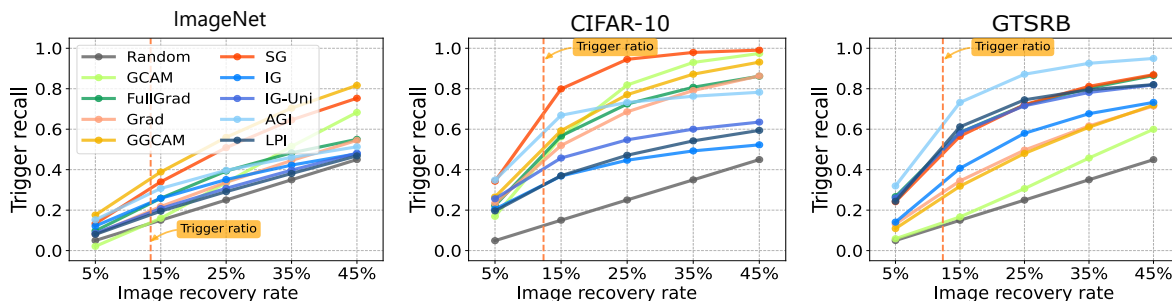


Fig. 10. Benchmarking of attribution methods under Blend attack using the trigger recall metric. Higher curves indicate better results.

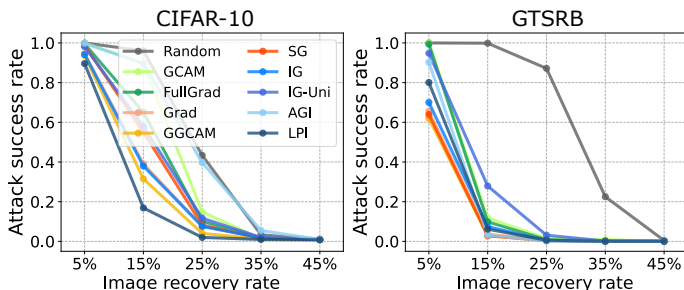


Fig. 11. Benchmarking of attribution methods under ISSBA attack using the attack success rate metric. Lower curves indicate better results.

6 BENCHMARKING

In this section, we conduct an extensive benchmarking of the attribution methods under BackX.

In Fig. 9, we provide results for Trojaned ResNet-18 models using the Blend attack with trigger visibility of 0.5. We employ nine attribution methods with varying image recovery rates across three datasets: ImageNet, CIFAR-10 and GTSRB. The corresponding trigger recall, as the image recovery rate increases, is reported in Fig. 10. Experimental results reveal that integration-based methods and gradient-based methods generally outperform CAM-based methods. Integration-based methods achieve superior performance on GTSRB, while gradient-based methods outperform others on CIFAR-10. Importantly, integration-based methods exhibit higher stability across different datasets.

It is observed that GGCAM significantly enhances CAM across all datasets with element-wise estimated attributions by incorporating Grad. Moreover, attribution methods estimated from perturbed inputs with steep slope curves, such as SG and AGI, demonstrate the best performance in locating important features. However, AGI’s random class

selection for calculating adversarial examples undermines its stability.

Figure 11 shows the attack success rate on a Trojaned model through ISSBA attack [25] on CIFAR-10 and GTSRB. Due to input-specific triggers demonstrating weak attack capabilities on larger-scale input samples, as they can be easily recovered by random attributions, we have excluded ImageNet from our experiments. Fine-grained integration-based and gradient-based methods can achieve outstanding performance for detecting invisible triggers. CAM-based methods, which fail to capture element-wise triggers, still manage to achieve competitive results compared to the integration-based and gradient-based methods.

In Fig. 12 and Fig. 14, we compare the fractional logit change for both the Blend and ISSBA attacks. The experimental results show the fractional change in logit output of both the true class y and the target class \tilde{y} to create a bubble chart. A faithful attribution method is expected to reduce the output of target class \tilde{y} while recovering the output of true class y . The markers representing different attribution methods are scaled by the corresponding performance. In this metric, integration-based methods exhibit both high performance and consistency. Additionally, compared to recovering the output of the true class y , all attribution methods are effective at decreasing the output of the target class \tilde{y} . Notably, CAM-based attribution methods can achieve competitive results in recovering the output of y compared to \tilde{y} , revealing the weak attack capability of invisible attacks. The results indicate that the attribution methods tend to perturb the target class rather than fully recover it. More results on fractional probability change and attribution visualizations are provided in Appx. 13. We make the following observation based on the overall results.

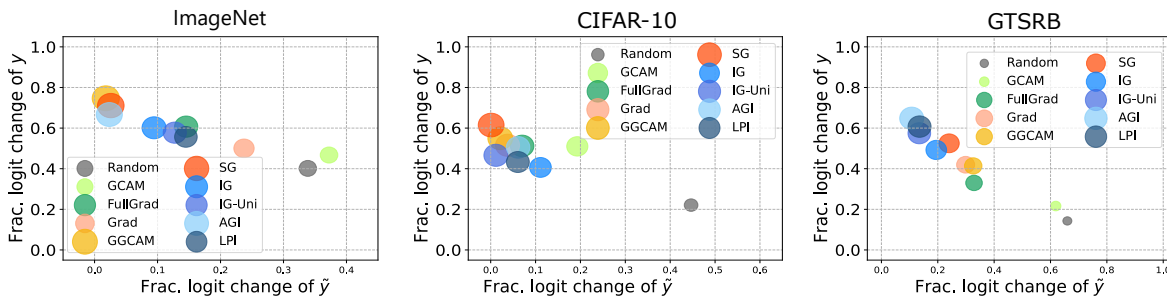


Fig. 12. Comparison of fractional logit change between attribution methods under Blend attack. Bubble size is scaled by the method’s performance. Approaching top-left corner in each plot indicates superior performance.

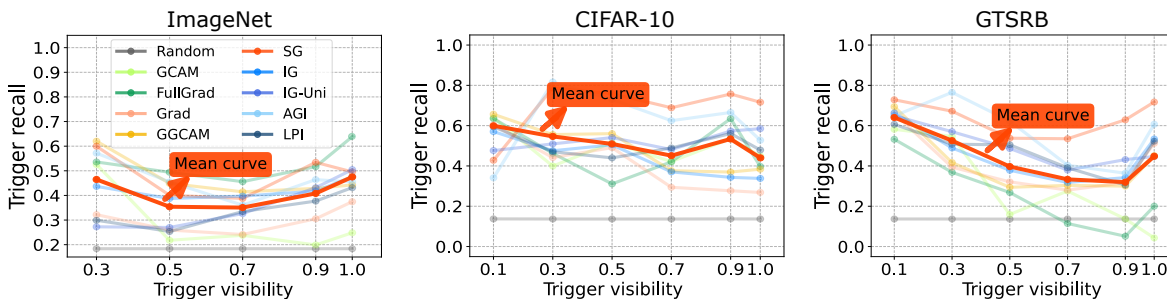


Fig. 13. Results of trigger recall changes with trigger visibility between attribution methods. Mean curves over various methods are highlighted. Higher trigger recall values correspond to an increased capacity to defend against backdoor attacks.

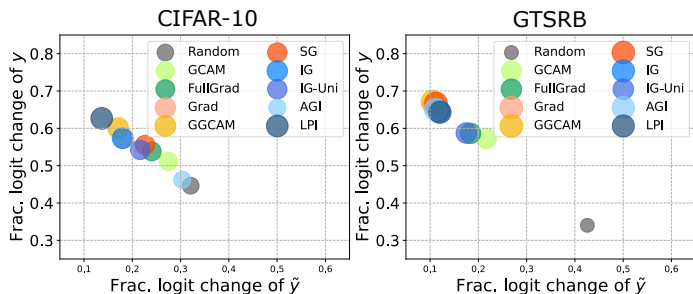


Fig. 14. Comparison of fractional logit change between attribution methods under ISSBA attack. Bubble size is scaled by the method’s performance. Approaching top-left corner in each plot indicates superior performance.

Observation 4

Gradient-based attribution methods tend to achieve better results, while integration-based methods exhibit more stability across different datasets. As compared to recovering the original class y , all attribution methods are better at reducing the misclassification to target \tilde{y} .

7 BACKDOOR DEFENSE WITH ATTRIBUTIONS

Here, we investigate the potential of the analyzed attribution methods for defending against backdoor attacks. In Fig. 13, we assess the change in attribution performance, measured by trigger recall, across varying trigger visibility. Counter to general intuition, we observe that attribution methods do not lead to better trigger localization with higher visibility of the trigger. This unanticipated behavior can be attributed to the fact that learning a robust feature, such as a clear trigger, does not demand fine-grained tuning of the model weights to attract its attention. In other words, better trigger visibility actually leads to a relatively easier

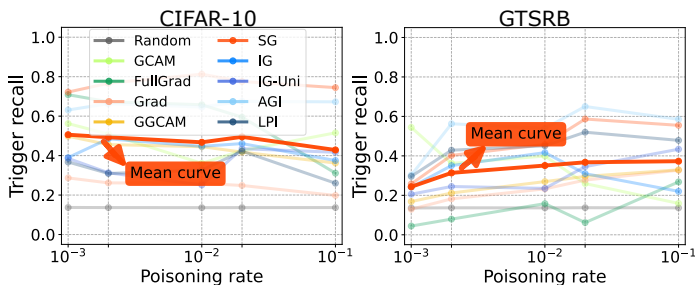


Fig. 15. Results of trigger recall changes with poisoning rate. Higher values correspond to better defense capability.

adversarial learning objective. Hence, trigger visibility fails to show a positive correlation with trigger recall through attribution. In Appx. 14.2, more visualization results of attribution maps are presented concerning the detection of triggers with varying degrees of visibility.

Figure 15 also reports the change in trigger recall as the poisoning rate varies. Interestingly, the poisoning rate also has only a limited effect on the performance of attribution methods. We provide more experimental results on defending backdoor attacks with attribution methods in Appx. 14. Based on our experiments, we make the following observation to provide guidance for employing attribution in defense against backdoor attacks.

Observation 5

Fixed or input-specific invisible attacks do not necessarily render defense more challenging. Fine-grained perturbation-based attribution methods, while incurring a higher computational cost, are more useful for backdoor defense. Additionally, CAM-based methods guided by fine-grained attributions are better choices for defense.

8 CONCLUSION

To establish a reliable benchmark for eXplainable Artificial Intelligence (XAI) in attribution methods, we devised a set of fidelity criteria aimed at assessing the evaluation faithfulness of such benchmarks. This facilitated a thorough comparison of existing benchmarks. Subsequently, a Backdoor-based evaluation framework (BackX) is developed, which underwent theoretical validation to ensure a superior level of fidelity criteria. Leveraging this fidelity benchmark, our study systematically explored various attribution methods, revealing their distinctive properties. This systematic exploration allowed for a consistent setup across different attribution methods, thereby mitigating confounding factors inherent in attribution estimation. Our framework employs this setup to conduct comprehensive benchmarking of attribution methods, highlighting both their strengths and weaknesses.

REFERENCES

- [1] K. He, X. Zhang, S. Ren, and J. Sun, "Deep residual learning for image recognition," in *IEEE Conference on Computer Vision and Pattern Recognition, CVPR*, 2016.
- [2] S. Ren, K. He, R. Girshick, and J. Sun, "Faster r-cnn: Towards real-time object detection with region proposal networks," *Advances in neural information processing systems, NeurIPS*, 2015.
- [3] I. Goodfellow, J. Pouget-Abadie, M. Mirza, B. Xu, D. Warde-Farley, S. Ozair, A. Courville, and Y. Bengio, "Generative adversarial nets," *Advances in neural information processing systems, NeurIPS*, 2014.
- [4] K. Gade, S. C. Geyik, K. Kenthapadi, V. Mithal, and A. Taly, "Explainable ai in industry," in *ACM SIGKDD Conference on Knowledge Discovery & Data Mining, KDD*, 2019.
- [5] E. Tjoa and C. Guan, "A survey on explainable artificial intelligence (xai): Toward medical xai," *IEEE Transactions on Neural Networks and Learning Systems, TNNLS*, vol. 32, no. 11, pp. 4793–4813, 2020.
- [6] K. Simonyan, A. Vedaldi, and A. Zisserman, "Deep inside convolutional networks: Visualising image classification models and saliency maps," in *International Conference on Learning Representations, ICLR*, 2014.
- [7] M. D. Zeiler and R. Fergus, "Visualizing and understanding convolutional networks," in *European Conference on Computer Vision, ECCV*, 2014.
- [8] M. Sundararajan, A. Taly, and Q. Yan, "Axiomatic attribution for deep networks," in *International Conference on Machine Learning, ICML*, 2017.
- [9] A. Shrikumar, P. Greenside, and A. Kundaje, "Learning important features through propagating activation differences," in *International Conference on Machine Learning, ICML*, 2017.
- [10] S. Srinivas and F. Fleuret, "Full-gradient representation for neural network visualization," in *Advances in Neural Information Processing Systems, NeurIPS*, 2019.
- [11] A. S. Ross, M. C. Hughes, and F. Doshi-Velez, "Right for the right reasons: Training differentiable models by constraining their explanations," in *International Joint Conference on Artificial Intelligence, IJCAI*, 2017.
- [12] X. Huang, M. Alzantot, and M. Srivastava, "Neuroninspect: Detecting backdoors in neural networks via output explanations," *CoRR*, vol. abs/1911.07399, 2019.
- [13] G. Erion, J. D. Janizek, P. Sturmfels, S. M. Lundberg, and S.-I. Lee, "Improving performance of deep learning models with axiomatic attribution priors and expected gradients," *Nature Machine Intelligence*, 2021.
- [14] S. Bach, A. Binder, G. Montavon, F. Klauschen, K.-R. Müller, and W. Samek, "On pixel-wise explanations for non-linear classifier decisions by layer-wise relevance propagation," *PloS one*, 2015.
- [15] W. Samek, A. Binder, G. Montavon, S. Lapuschkin, and K.-R. Müller, "Evaluating the visualization of what a deep neural network has learned," *IEEE Transactions on Neural Networks and Learning Systems, TNNLS*, 2016.
- [16] V. Petsiuk, A. Das, and K. Saenko, "RISE: randomized input sampling for explanation of black-box models," in *British Machine Vision Conference, BMVC*, 2018.
- [17] Y. Rong, T. Leemann, V. Borisov, G. Kasneci, and E. Kasneci, "A consistent and efficient evaluation strategy for attribution methods," in *International Conference on Machine Learning, ICML*, 2022.
- [18] S. Hooker, D. Erhan, P. Kindermans, and B. Kim, "A benchmark for interpretability methods in deep neural networks," in *Advances in Neural Information Processing Systems, NeurIPS*, 2019.
- [19] J. Zhang, S. A. Bargal, Z. Lin, J. Brandt, X. Shen, and S. Sclaroff, "Top-down neural attention by excitation backprop," *International Journal of Computer Vision, IJCV*, 2018.
- [20] S. Rao, M. Böhle, and B. Schiele, "Towards better understanding attribution methods," in *IEEE Conference on Computer Vision and Pattern Recognition, CVPR*, 2022.
- [21] L. Arras, A. Osman, and W. Samek, "Clevr-xai: A benchmark dataset for the ground truth evaluation of neural network explanations," *Information Fusion*, vol. 81, pp. 14–40, 2022.
- [22] Y.-S. Lin, W.-C. Lee, and Z. B. Celik, "What do you see? evaluation of explainable artificial intelligence (xai) interpretability through neural backdoors," in *ACM SIGKDD Conference on Knowledge Discovery & Data Mining, KDD*, 2021, pp. 1027–1035.
- [23] T. Gu, K. Liu, B. Dolan-Gavitt, and S. Garg, "Badnets: Evaluating backdooring attacks on deep neural networks," *IEEE Access*, vol. 7, pp. 47 230–47 244, 2019.
- [24] X. Chen, C. Liu, B. Li, K. Lu, and D. Song, "Targeted backdoor attacks on deep learning systems using data poisoning," *CoRR*, vol. abs/1712.05526, 2019.
- [25] Y. Li, Y. Li, B. Wu, L. Li, R. He, and S. Lyu, "Invisible backdoor attack with sample-specific triggers," in *IEEE Conference on Computer Vision and Pattern Recognition, CVPR*, 2021.
- [26] D. Smilkov, N. Thorat, B. Kim, F. Viégas, and M. Wattenberg, "Smoothgrad: removing noise by adding noise," *CoRR*, vol. abs/1706.03825, 2017.
- [27] Y. Wang and X. Wang, "'why not other classes?': Towards class-contrastive back-propagation explanations," *Advances in Neural Information Processing Systems, NeurIPS*, 2022.
- [28] P. Yang, N. Akhtar, Z. Wen, M. Shah, and A. S. Mian, "Recalibrating feature attributions for model interpretation," in *International Conference on Learning Representations, ICLR*, 2023.
- [29] T. Han, S. Srinivas, and H. Lakkaraju, "Which explanation should i choose? a function approximation perspective to characterizing post hoc explanations," *Advances in Neural Information Processing Systems, NeurIPS*, 2022.
- [30] J. T. Springenberg, A. Dosovitskiy, T. Brox, and M. A. Riedmiller, "Striving for simplicity: The all convolutional net," in *International Conference on Learning Representations, ICLR*, 2015.
- [31] B. Zhou, A. Khosla, A. Lapedriza, A. Oliva, and A. Torralba, "Learning deep features for discriminative localization," in *IEEE Conference on Computer Vision and Pattern Recognition, CVPR*, 2016.
- [32] R. R. Selvaraju, M. Cogswell, A. Das, R. Vedantam, D. Parikh, and D. Batra, "Grad-cam: Visual explanations from deep networks via gradient-based localization," in *International Conference on Computer Vision, ICCV*, 2017.
- [33] P. Sturmfels, S. Lundberg, and S.-I. Lee, "Visualizing the impact of feature attribution baselines," *Distill*, 2020.
- [34] D. Pan, X. Li, and D. Zhu, "Explaining deep neural network models with adversarial gradient integration," in *International Joint Conference on Artificial Intelligence, IJCAI*, 2021.
- [35] N. Akhtar and M. A. Jalwana, "Towards credible visual model interpretation with path attribution," in *International Conference on Machine Learning*. PMLR, 2023, pp. 439–457.
- [36] H. Shah, P. Jain, and P. Netrapalli, "Do input gradients highlight discriminative features?" *Advances in Neural Information Processing Systems, NeurIPS*, 2021.
- [37] P. Yang, N. Akhtar, Z. Wen, and A. Mian, "Local path integration for attribution," in *AAAI Conference on Artificial Intelligence, AAAI*, 2023.
- [38] M. Ancona, E. Ceolini, C. Öztireli, and M. Gross, "Towards better understanding of gradient-based attribution methods for deep neural networks," in *International Conference on Learning Representations, ICLR*, 2018.
- [39] C.-K. Yeh, C.-Y. Hsieh, A. Suggala, D. I. Inouye, and P. K. Ravikumar, "On the (in) fidelity and sensitivity of explanations," *Advances in Neural Information Processing Systems, NeurIPS*, 2019.

- [40] J. Adebayo, J. Gilmer, M. Mueley, I. J. Goodfellow, M. Hardt, and B. Kim, "Sanity checks for saliency maps," in *Advances in Neural Information Processing Systems, NeurIPS*, 2018.
- [41] A. Khakzar, P. Khorsandi, R. Nobahari, and N. Navab, "Do explanations explain? model knows best," in *IEEE Conference on Computer Vision and Pattern Recognition, CVPR*, 2022.
- [42] A. Nguyen and A. Tran, "Wanet-imperceptible warping-based backdoor attack," *International Conference on Learning Representations, ICLR*, 2021.
- [43] X. Qi, T. Xie, Y. Li, S. Mahloujifar, and P. Mittal, "Revisiting the assumption of latent separability for backdoor defenses," in *International Conference on Learning Representations, ICLR*, 2022.
- [44] E. Chou, F. Tramer, and G. Pellegrino, "Sentinet: Detecting localized universal attacks against deep learning systems," in *IEEE Security and Privacy Workshops, SPW*, 2020.
- [45] A. Turner, D. Tsipras, and A. Madry, "Label-consistent backdoor attacks," *CoRR*, vol. abs/1912.02771, 2019.
- [46] W. Guo, B. Tondi, and M. Barni, "An overview of backdoor attacks against deep neural networks and possible defences," *IEEE Open Journal of Signal Processing*, 2022.
- [47] C. Szegedy, W. Zaremba, I. Sutskever, J. Bruna, D. Erhan, I. Goodfellow, and R. Fergus, "Intriguing properties of neural networks," *arXiv preprint arXiv:1312.6199*, 2013.
- [48] N. Hoque, D. K. Bhattacharyya, and J. K. Kalita, "Mifs-nd: A mutual information-based feature selection method," *Expert Systems with Applications*, vol. 41, no. 14, pp. 6371–6385, 2014.
- [49] P.-T. Jiang, C.-B. Zhang, Q. Hou, M.-M. Cheng, and Y. Wei, "Layercam: Exploring hierarchical class activation maps for localization," *IEEE Transactions on Image Processing, TIP*, vol. 30, pp. 5875–5888, 2021.
- [50] M. B. Muhammad and M. Yeasin, "Eigen-cam: Class activation map using principal components," in *International Joint Conference on Neural Networks, IJCNN*, 2020.
- [51] M. T. Ribeiro, S. Singh, and C. Guestrin, "Why should I trust you?" explaining the predictions of any classifier," in *ACM SIGKDD Conference on Knowledge Discovery & Data Mining, KDD*, 2016.
- [52] S. M. Lundberg and S.-I. Lee, "A unified approach to interpreting model predictions," in *Advances in Neural Information Processing Systems, NeurIPS*, 2017.
- [53] R. C. Fong and A. Vedaldi, "Interpretable explanations of black boxes by meaningful perturbation," in *International Conference on Computer Vision, ICCV*, 2017.
- [54] A. Binder, G. Montavon, S. Lapuschkin, K.-R. Müller, and W. Samek, "Layer-wise relevance propagation for neural networks with local renormalization layers," in *International Conference on Artificial Neural Networks, ICANN*, 2016.
- [55] A. Krizhevsky, G. Hinton *et al.*, "Learning multiple layers of features from tiny images," *Technical Report, University of Toronto*, 2009.
- [56] S. Houben, J. Stallkamp, J. Salmen, M. Schlipsing, and C. Igel, "Detection of traffic signs in real-world images: The german traffic sign detection benchmark," in *International Joint Conference on Neural Networks, IJCNN*, 2013.
- [57] O. Russakovsky, J. Deng, H. Su, J. Krause, S. Satheesh, S. Ma, Z. Huang, A. Karpathy, A. Khosla, M. Bernstein *et al.*, "Imagenet large scale visual recognition challenge," *International Journal of Computer Vision*, vol. 115, no. 3, pp. 211–252, 2015.
- [58] J. R. Vergara and P. A. Estévez, "A review of feature selection methods based on mutual information," *Neural computing and applications*, vol. 24, pp. 175–186, 2014.



Peiyu Yang is currently pursuing a doctoral degree at The University of Western Australia. Prior to this, he received a Master's degree from Northeastern University, Shenyang, China, in 2020. His primary research interests center around explainable artificial intelligence and trustworthy machine learning, with a focus on feature attributions, robust regularization, neural Trojans, and adversarial learning.



Naveed Akhtar is a Senior Lecturer at the University of Melbourne. He received his PhD in Computer Science from the University of Western Australia and Master degree from Hochschule Bonn-Rhein-Sieg, Germany. He is a recipient of the Discovery Early Career Researcher Award from the Australian Research Council. He is a Universal Scientific Education and Research Network Laureate in Formal Sciences. He was a finalist of the Western Australia's Early Career Scientist of the Year 2021.

He is an ACM Distinguished Speaker and serves as an Associate Editor of IEEE Trans. Neural Networks and Learning Systems.



Jiantong Jiang is currently a PhD candidate at The University of Western Australia, after receiving a Master's degree from Northeastern University in China. Before commencing her PhD study, she was a Research Assistant at School of Software Engineering, Zhejiang University, China. Her research interests include high-performance computing and automatic machine learning system.



Ajmal Mian is a Professor of Computer Science at the University of Western Australia. He is the recipient of three prestigious national level fellowships from the Australian Research Council (ARC) including the recent Future Fellowship award 2022. He is a Fellow of the International Association for Pattern Recognition, Distinguished Speaker of the Association for Computing Machinery and President of the Australian Pattern Recognition Society. He received the West Australian Early Career Scientist of the

Year Award 2012 and the HBF Mid-Career Scientist of the Year Award 2022. He has secured research funding from the ARC, the National Health and Medical Research Council of Australia, US Department of Defence DARPA, and the Australian Department of Defence. He has published over 260 scientific papers. He is a Senior Editor for IEEE TNNLS and Associate Editor IEEE TIP and the Pattern Recognition journal. His research interests include computer vision, artificial intelligence, deep learning, 3D point cloud analysis, facial recognition, human action measurement and video analysis.

Backdoor-based Explainable AI Benchmark for High Fidelity Evaluation of Attribution Methods

Appendix

9 NOTATION

In Table 2, we provide a summary of the notations used in the paper, along with their corresponding definitions.

10 PROOF

In this section, we provide the proof of Proposition 1 and Proposition 2.

Proof of Proposition 1. Assuming that $\tilde{\epsilon}$ is a subset of ϵ , any deviation from the original data distribution caused by the poisoned sample \tilde{x} is constrained within the boundary of ϵ . The recovery process aims to undo the perturbation introduced by the poisoned sample \tilde{x} . By constraining the transformation from \tilde{x} to \hat{x} such that $\Omega(x, \hat{x}) \leq \Omega(x, \tilde{x})$, the recovered sample \hat{x} can be ensured to remain within the boundary defined by ϵ . Therefore, under the condition that $\tilde{\epsilon} \leq \epsilon$, the recovery process preserves the original data distribution, and the recovered sample \hat{x} is preserved within the original distribution. Thus, if $\tilde{\epsilon} \leq \epsilon$, the recovered sample \hat{x} is preserved within the original data distribution. \square

Proof of Proposition 2. Given a recovery image \hat{x} , the performance of attribution methods for a target class c evaluated in our BackX benchmark can be represented as $I(\hat{x}; c)$. We follow the derivation on the multi-information as Vergara & Estévez [58], Rong et al. [17]. Assume an attribution mask S , the multi-information $I(\hat{x}; c; M)$ can be represented as

$$I(c; \hat{x}|S) = I(c; \hat{x}|S) - I(\hat{x}; c), \quad (11)$$

$$I(\hat{x}; c; S) = I(c; S|\hat{x}) - I(S; c). \quad (12)$$

By equating Equation 11 and Equation 12, we can derive

$$I(\hat{x}; c) = I(c; \hat{x}|S) + I(S; c) - I(c; S|\hat{x}), \quad (13)$$

where $I(c; \hat{x}|S)$ represents the target we aim to estimate, representing the mutual information between the recovery input \hat{x} and a class c for a given mask S . $I(S; c)$ represents the mutual information between S and c , which we aim to eliminate. The last term $I(c; S|\hat{x})$ indicates mutual information between S and c given \hat{x} , compensating for $I(S; c)$.

Minimizing the mutual information $I(S; c)$ between the mask and the class label leads to the approximation that $I(S; c)$ approaches $I(c; S|\hat{x})$, specifically $I(S; c) \approx I(c; S|\hat{x})$. Thus, this mitigation of the leaked information $I(S; c)$ from the mask S leads to an improvement in the reliability of the evaluation results for $I(\hat{x}; c)$, specifically $I(\hat{x}; c) \approx I(c; \hat{x}|S)$. \square

11 EXPERIMENTAL SETUP

In this section, we present a comprehensive experimental setup and hyperparameter choice for Trojaned models and benchmarked attribution methods, as well as details of the used experimental software and platform.

11.1 Trigger Patterns and Poisoned Samples

In our BackX benchmark, we incorporate both visible and invisible trigger patterns to provide a comprehensive evaluation, which allows us to thoroughly assess the capability of attribution methods in detecting both fixed visible patterns and input-specific invisible triggers. Figure 16 provides examples of the trigger patterns utilized in our

TABLE 2
The used notations and the corresponding definition.

Notation	Definition
$x, \tilde{x} \in \mathbb{R}^n$	Input clean sample and poisoned sample within a n -dimensional input space
$y, \tilde{y} \in \mathbb{R}^c$	True label and target label within a c -dimensional output space
f, \tilde{f}	Clean benign model and Trojaned model
$f(x), p(x)$	Output logits and output probabilities
ϕ	Attribution method
M, M^*	Estimated attributions and attribution ground truth
ζ	Perturbation operator for model
ξ	Perturbation operator for input
$\mathcal{D}, \tilde{\mathcal{D}}$	Training set and poisoned training set
$\mathcal{P}_{\mathcal{D}}$	Input distribution
$S^{(k)}, S^* \in \{0, 1\}^n$	Attribution mask indicating $k\%$ most important elements and a mask of a trigger pattern
\hat{x}	Recovery sample
x'	Reference input
$\nabla_x f(x)$	Input gradients of output logits
v	Trigger pattern
α	Trigger visibility
$\mathbf{I}(\cdot)$	Bool function
$H(\cdot)$	Entropy of a variable
$I(\cdot)$	Mutual information between variables
$A_{i,j}^k$	$(i$ -th, j -th) element of activations in k -th layer
w_k^c	activation weight of c -th class in k -th layer
Ψ	Interpolated operator

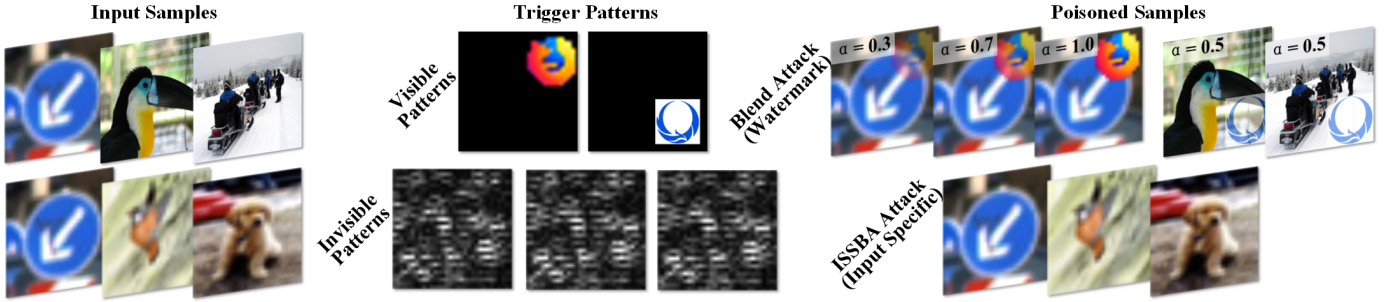


Fig. 16. Illustrations of input samples, trigger patterns and poisoned samples. The top arrow depicts fixed trigger patterns and corresponding poisoned samples with triggers in varying visibility (α) used in the Blend attack. The bottom arrow illustrates invisible input-specific trigger patterns and corresponding poisoned samples generated using the ISSBA attack.

TABLE 3

Comparison of accuracy among various ResNet-18 models Trojaned through Blend attack with triggers of varying visibility on CIFAR-10. The accuracy of the benign model (N/A) is also reported.

Test set	Trigger visibility (α)						
	N/A	0.1	0.3	0.5	0.7	0.9	1.0
Poisoned	0.008	0.993	0.999	1.000	1.000	1.000	1.000
Clean	0.943	0.936	0.933	0.928	0.935	0.937	0.933

TABLE 4

Comparison of accuracy among various ResNet-18 models Trojaned through Blend attack with triggers of varying visibility on GTSRB. The accuracy of the benign model (N/A) is also reported.

Test set	Trigger visibility (α)						
	N/A	0.1	0.3	0.5	0.7	0.9	1.0
Poisoned	0.001	0.992	0.999	1.000	1.000	1.000	1.000
Clean	0.973	0.967	0.965	0.970	0.971	0.967	0.969

TABLE 5

Comparison of accuracy among various ResNet-34 models Trojaned through Blend attack with triggers of varying visibility on ImageNet. The accuracy of the benign model (N/A) is also reported.

Test set	Trigger visibility (α)					
	N/A	0.3	0.5	0.7	0.9	1.0
Poisoned	0.000	0.987	0.998	0.995	0.999	1.000
Clean	0.724	0.713	0.717	0.715	0.714	0.716

TABLE 6

Comparison of accuracy among various ResNet-18 models Trojaned through Blend attack with different poisoning rates on CIFAR-10.

Test set	Poisoning rate				
	0.001	0.005	0.01	0.05	0.1
Poisoned	0.975	1.000	0.999	1.000	1.000
Clean	0.937	0.938	0.936	0.939	0.928

TABLE 7

Comparison of accuracy among various ResNet-18 models Trojaned through Blend attack with different poisoning rates on GTSRB.

Test set	Poisoning rate				
	0.001	0.005	0.01	0.05	0.1
Poisoned	0.745	0.997	0.998	1.000	1.000
Clean	0.969	0.966	0.971	0.970	0.970

experiments and the corresponding poisoned samples. In the Blend attack [24], we utilize fixed visible trigger patterns, consistent with Qi et al. [43]. In addition, we employ a pre-trained encoder network to generate input-specific invisible trigger patterns in the ISSBA attack [25]. The trigger patterns used in these attacks are depicted in the middle column of Figure 16. Given a set of input samples, as shown in the first column of Figure 16, the resulting poisoned samples are presented in the last column of Figure 16.

11.2 Performance Comparison of Explained Models

In this part, we show the detailed performance of used models trained on different datasets. For all the Trojaned models under comparison, we select the target label as the first class for a single target backdoor attack on both the CIFAR-10 and ImageNet datasets, and the third class for the GTSRB dataset followed by Qi et al. [43].

Tables 3 and 4 display the accuracy comparison of Trojaned ResNet-18 models as the visibility of the Trojan trigger varies on the CIFAR-10 and GTSRB datasets. Similarly, Table 5 compares the accuracy of different Trojaned ResNet-32 models on ImageNet. In all cases, a consistent poisoning rate of 0.1 was employed during model Trojaning. Notably, these tables illustrate that changes in trigger visibility do not lead to a marked decrease in accuracy on the clean dataset. Additionally, there is a minor reduction in accuracy on the poisoned dataset to ensure a fair comparison. These results provide compelling evidence that a sample containing the Trojan trigger can completely alter the model's predictions, providing the ground truth of attributions. The first column in each table compares the accuracy of the benign model on the respective datasets, highlighting that Trojaned models only exhibit a slight performance compromise compared to their benign counterparts.

TABLE 8
Comparison of accuracy among various ResNet-18 models Trojaned through ISSBA attack on CIFAR-10 and GTSRB.

Test set	Dataset	
	CIFAR-10	GTSRB
Poisoned	1.000	1.000
Clean	0.938	0.972

Table 6 and Table 7 present the accuracy changes in models Trojaned with different poisoning rates, ranging from 0.001 to 0.1, on the CIFAR-10 and GTSRB datasets. These tables demonstrate that models Trojaned with various poisoning rates only result in a subtle reduction in clean accuracy. It enables our experiments to maintain relatively consistent accuracy levels across different poisoning rates.

In Table 8, we show the accuracy comparison of ResNet models Trojaned through the ISSBA attack with a poisoning rate of 0.05 on both CIFAR-10 and GTSRB datasets. We have ensured consistent standard accuracy and high accuracy on the poisoned dataset to enable a fair comparison. Furthermore, Table 9 compares accuracy on both the poisoned and clean datasets across three different models.

The results highlight that Trojaned models exhibit the ability to adapt and fit the input distribution when optimizing the poisoned samples. As these Trojaned models converge during training on these samples, we are now equipped with the capacity to conduct a comprehensive and rigorous evaluation of attribution methods specifically within the context of Trojaned models. While other studies have demonstrated the presence of feature disparities in the hidden layers of Trojaned models within the latent space [43], our findings suggest that these models can still be considered reliable for evaluating explanations related to the model’s output layer. However, further exploring the impact of the disparity in evaluating attribution methods is left in our future work.

11.3 Hyperparameter Choice

1) *Model Training and Evaluation:* In our experiments, we trained ResNet-18 on CIFAR-10 for 100 epochs, starting with an initial learning rate of 0.1. We applied a learning rate decay by a factor of 10 at the 50-th and 75-th epochs separately. On GTSRB, ResNet-18 was trained for a total of 100 epochs, with a learning rate of 0.1, and we applied a learning

TABLE 9
Accuracy comparison of ResNet-18, ResNet-32, ResNet-50 and ResNet-101 models Trojaned through Blend attack on ImageNet.

Test set	Model			
	ResNet-18	ResNet-34	ResNet-50	ResNet-101
Poisoned	0.998	0.998	0.993	0.990
Clean	0.682	0.717	0.728	0.749

rate decay at the 30-th and 60-th epochs. Additionally, we trained ResNet-18, ResNet-34, ResNet-50, and ResNet-101 on ImageNet 2012 training set for a total of 90 epochs, with an initial learning rate of 10^{-2} , which was decayed at the 30-th and 60-th epochs. This setup was consistent for models subjected to both Blend attack and ISSBA attack. In the benchmarking, we use the test sets of both the CIFAR-10 and GTSRB datasets. For the ImageNet 2012 dataset, attribution methods are assessed on the ImageNet 2012 Validation set.

2) *Attribution Methods:* In our experiments, we test three groups of attribution methods including CAM-based, gradient-based and integration-based attribution methods. In two **CAM-based attribution methods**, GCAM and FullGrad, we remove the ReLU layer that is typically applied in activation calculation, ensuring the original activations. In addition, we applied two CAM-based attributions to explain model output probabilities. For all **gradient-based attribution methods**, the attributions are calculated by explaining output logits. In addition, we take the absolute values of the calculated attributions of gradient-based methods. In SG, we integrate gradients of 50 perturbed input samples that are added Gaussian noise with a standard deviation of 0.15. In **integrated-based attribution methods**, we retain the original values of estimated attributions by explaining output probabilities. Specifically, we sample 50 interpolations \bar{x} from the reference x' to the input x in IG for attribution estimation. In IG-Uni, IG-SG and LPI, we employ 10 references and 5 interpolations to maintain the same total number of interpolations of 50 for a fair comparison. Specifically, IG-SG employs the same deviation in Gaussian noise as SG. References of LPI are sampled from the training set by one central clustering. In contrast, we select 5 references and 10 interpolations in AGI for a higher performance due to its reliance on more interpolation points for estimating adversarial examples.

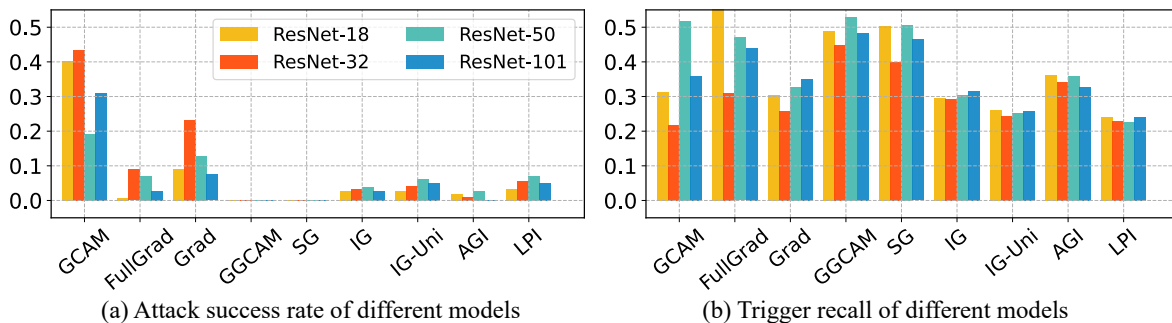


Fig. 17. The comparison of (a) attack success rate and (b) trigger recall across different model architectures using different attribution methods on ImageNet. A **lower** attack success rate indicates **better** results, while a **higher** trigger recall indicates **better** results.

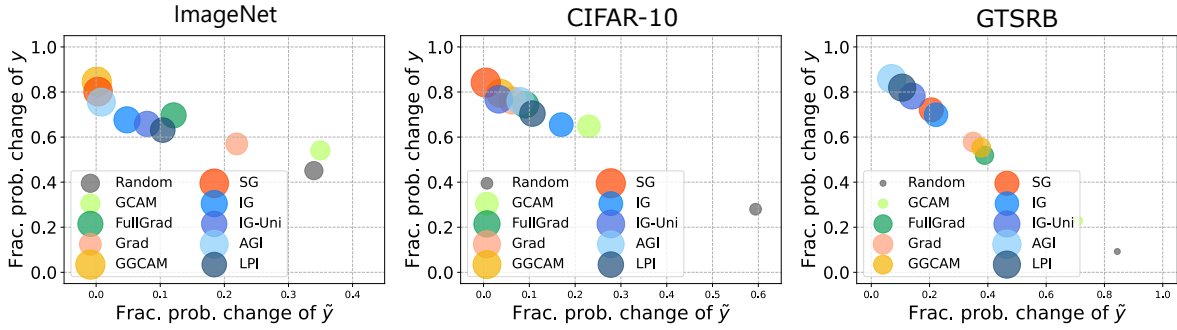


Fig. 18. The comparison of fractional probability change under Blend attack. Different attribution methods are scaled according to their performance. Approaching top-left corner in each plot indicates superior performance.

11.4 Experimental Software and Platform

All experiments were performed on a Linux-based system equipped with an NVIDIA GTX 3090Ti GPU boasting 24GB of memory, complemented by a 16-core 3.9GHz Intel Core i9-12900K CPU and 128GB of main memory. For both testing and training purposes, all attribution methods were implemented and evaluated within the PyTorch deep learning framework (version 1.12.1), utilizing the Python programming language.

12 EXPERIMENTS OF MODEL ARCHITECTURES

In Figure 17, we conduct a comparison of both attack success rate and trigger recall across different model architectures using various attribution methods. All three models were trained on ImageNet with a Trojan trigger of 0.5 visibility and a 0.1 poisoning rate. Table 9 shows the detailed performance comparison of the three models. It can be observed that two CAM-based attribution methods and Grad exhibit sensitivity to changes in model architecture, indicating weaker stability. Conversely, most attribution methods show consistent performance across varying model architectures, demonstrating a stable behavior.

13 EXTENDED EXPERIMENTS OF OVERALL BENCHMARKS

In this part, we provide more overall benchmarking experimental results. In addition, more visualization examples are presented for a visual inspection.

13.1 Results of Fractional Probability Change.

Figure 18 and Figure 19 presents a comparison of fractional probability change across attribution methods for both Blend and ISSBA attacks. It is evident that gradient-based and integration-based attribution methods consistently exhibit the highest performance and stability in reducing the output of \hat{y} and recovering the output of y . CAM-based methods, including GGCAM, also demonstrate high performance, relying on a combination of fine-grained attributions.

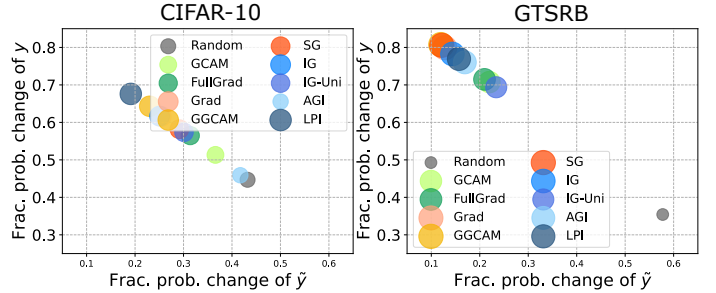


Fig. 19. The comparison of fractional probability change under ISSBA attack. Different attribution methods are scaled according to their performance. Approaching top-left corner in each plot indicates superior performance.

13.2 Visual Inspection of Attributions

In Figure 22 and Figure 23, we provide visualization examples for explaining models Trojaned through Blend attack using attribution methods across three datasets: CIFAR-10, GTSRB and ImageNet. Three groups of attribution methods are compared including CAM-based, Gradient-based and Integration-based methods. In the visualization experiments, original attributions of output logits are used in CAM-based and integration-based attribution methods. In addition, absolute attributions of output probabilities are visualized in gradient-based attribution methods as the established consistent setup. It can be observed that absolute attributions are good at generating plausible visualization examples. Similar to our observation, GCAM relies on other information to generate fine-grained attributions (e.g. FG and GGCAM).

Figure 24 presents visualization examples for explaining ResNet-18 models Trojaned through ISSBA attack using attribution methods of three groups on both CIFAR-10 and GTSRB datasets. We can observe that attributions with high variations are also effective in identifying invisible patterns in comparison with fixed patterns.

14 EXTENDED EXPERIMENTS OF BACKDOOR DEFENSE

In this part, more experiments are provided for defending against backdoor attacks using attribution methods. In addition, more visualization examples for detecting various triggers are provided for visual inspection.

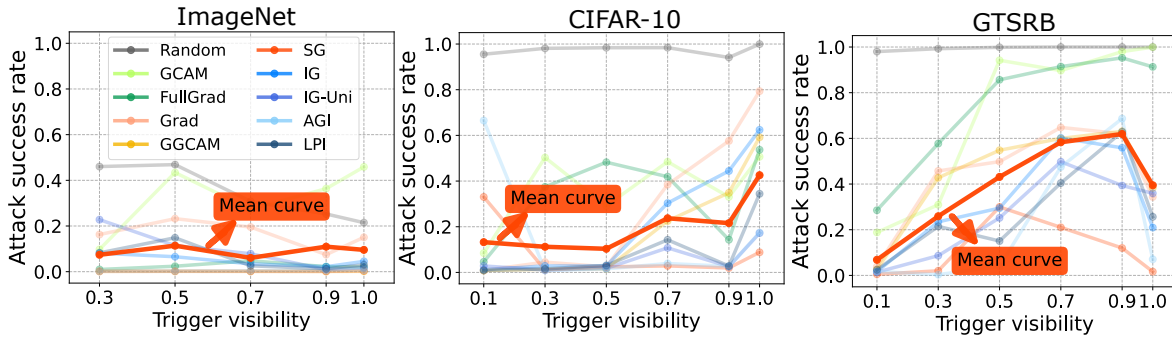


Fig. 20. The results of attack success rate. Trigger recall changes as trigger visibility. Mean curves over various methods are highlighted. Lower values of attack success rate correspond to an increased capacity to defend against backdoor attacks.

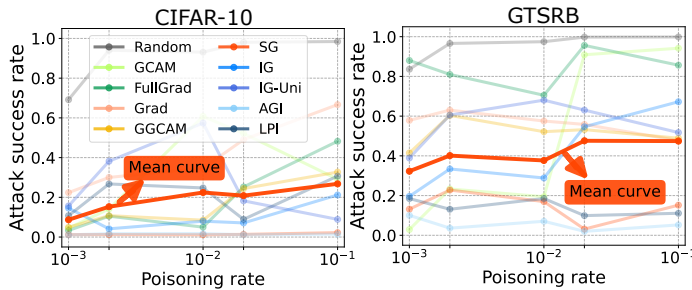


Fig. 21. The results of attack success rate. Trigger recall changes as poisoning rate. Mean curves over various methods are highlighted. Lower values of attack success rate correspond to an increased capacity to defend against backdoor attacks.

14.1 Results of Attack Success Rate.

In Figure 20 and Figure 21, we compare the results of attack success rate on models Trojanned through Blend attack with different trigger visibilities and poisoning rates. It can be observed that the visibility of the trigger is not positively related to attribution performance. In contrast, the higher visibility trigger sometimes causes a higher attack success rate, which aligns with our observation. In addition, different poisoning rates show less impact on the ease of defense, as shown in Figure 21.

14.2 Visual Inspection for Backdoor Attack

In Figure 25, we undertake an evaluation of attribution performance concerning the detection of triggers with varying degrees of visibility. Contrary to our intuitive assumptions, we observe that attribution methods encounter increased difficulty in identifying triggers with higher visibility, a trend that aligns with our empirical findings. This discovery prompts us to reconsider our intuition about feature learning within model optimization processes.

Figure 26 presents visualization examples of attribution maps with changes in the poisoning rate. Notably, it is apparent that attributions exhibit a relatively minimal influence on models subjected to different poisoning rates. This observation underscores the resilience of model behavior to alterations induced by varying levels of poisoning, highlighting the intricate dynamics at play in adversarial model manipulation.

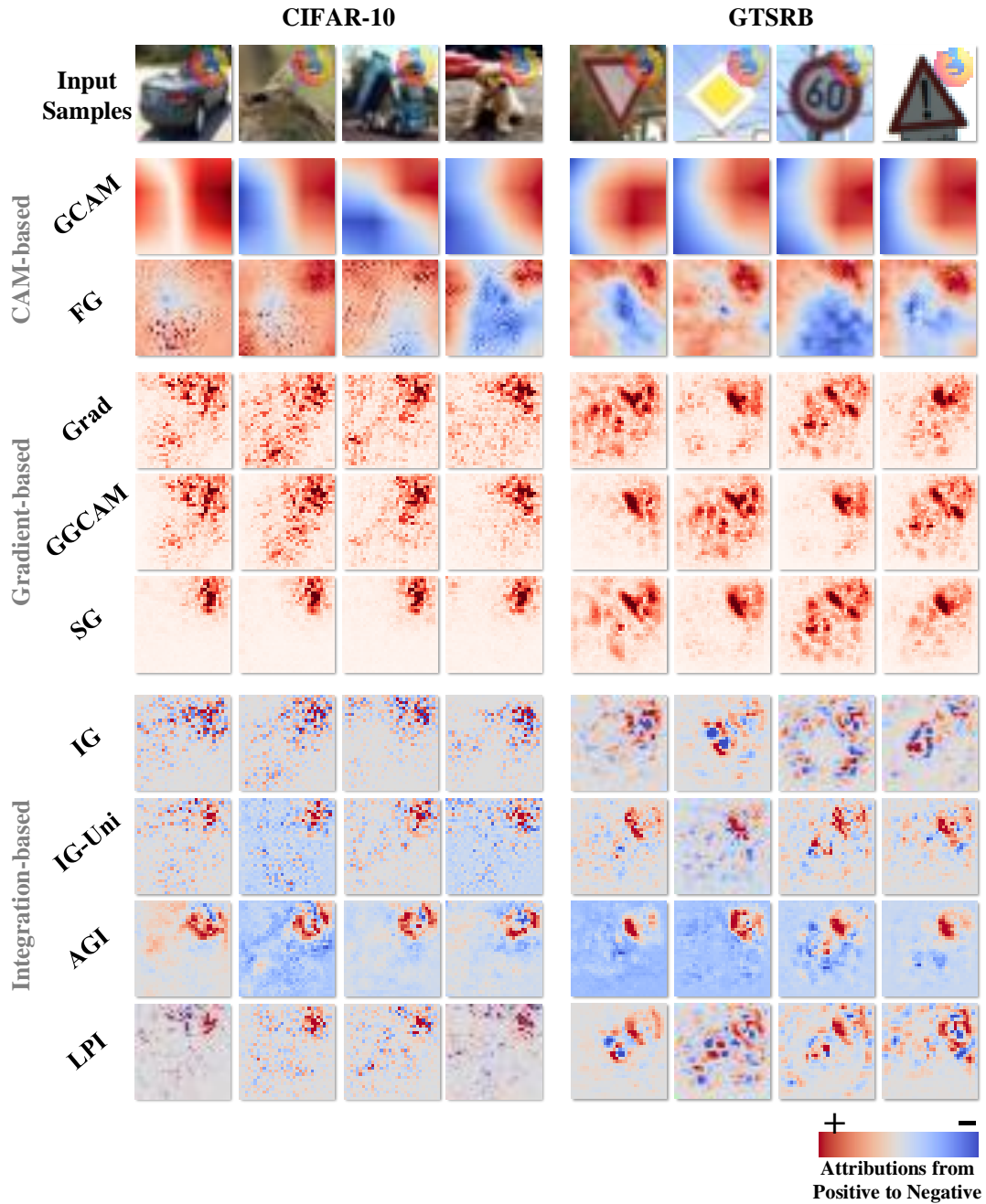


Fig. 22. Visual comparison of attribution methods on CIFAR-10 and GTSRB datasets. Predictions made by ResNet-18 models Trojaned through the Blend attack with a trigger visibility of 0.5 are explained using three groups of attribution methods including CAM-based, Gradient-based, and Integration-based methods.

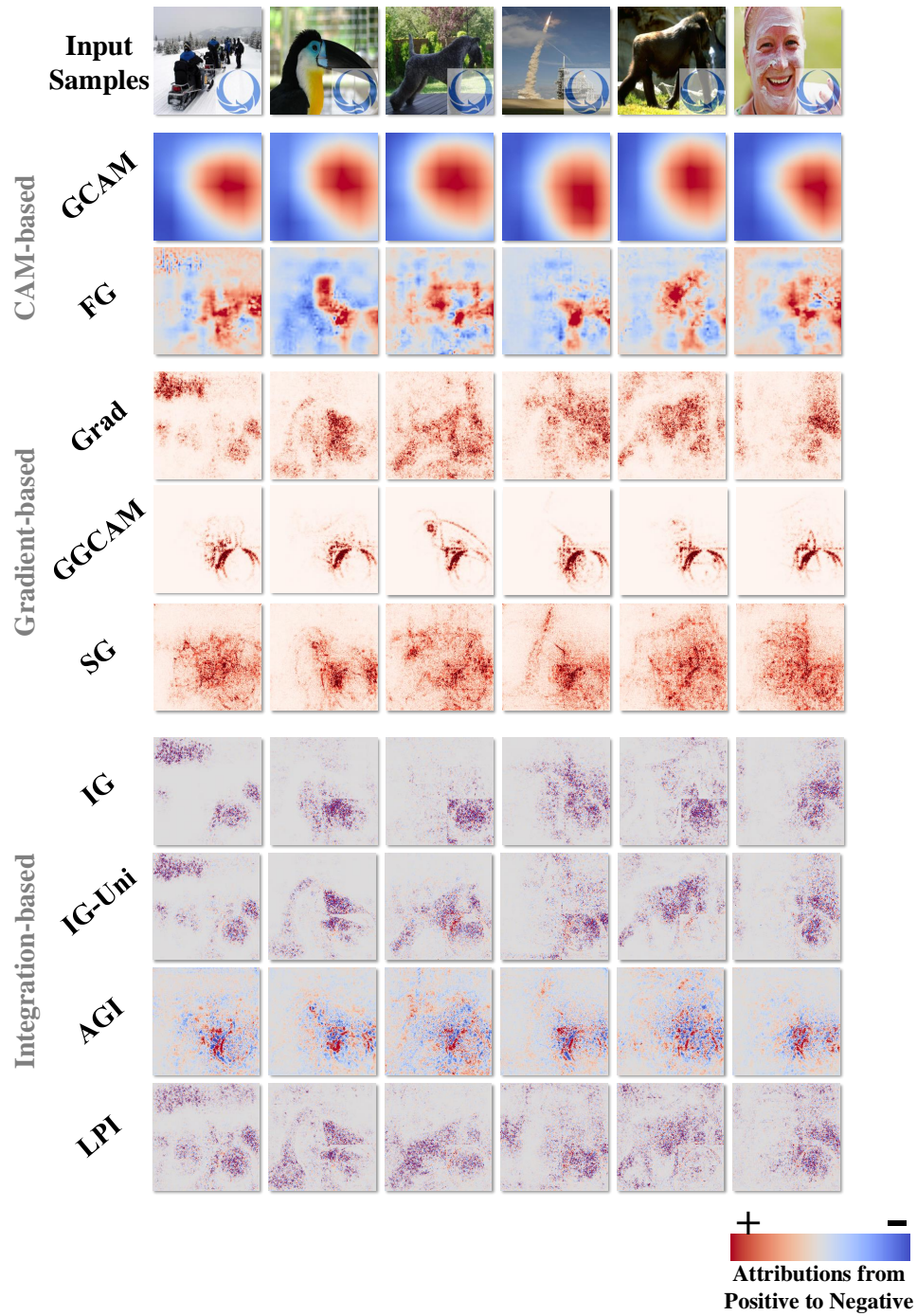


Fig. 23. Visual comparison of attribution methods on ImageNet 2012. Predictions made by ResNet-34 models Trojanned through the Blend attack with a trigger visibility of 0.5 are explained using three groups of attribution methods including CAM-based, Gradient-based, and Integration-based methods.

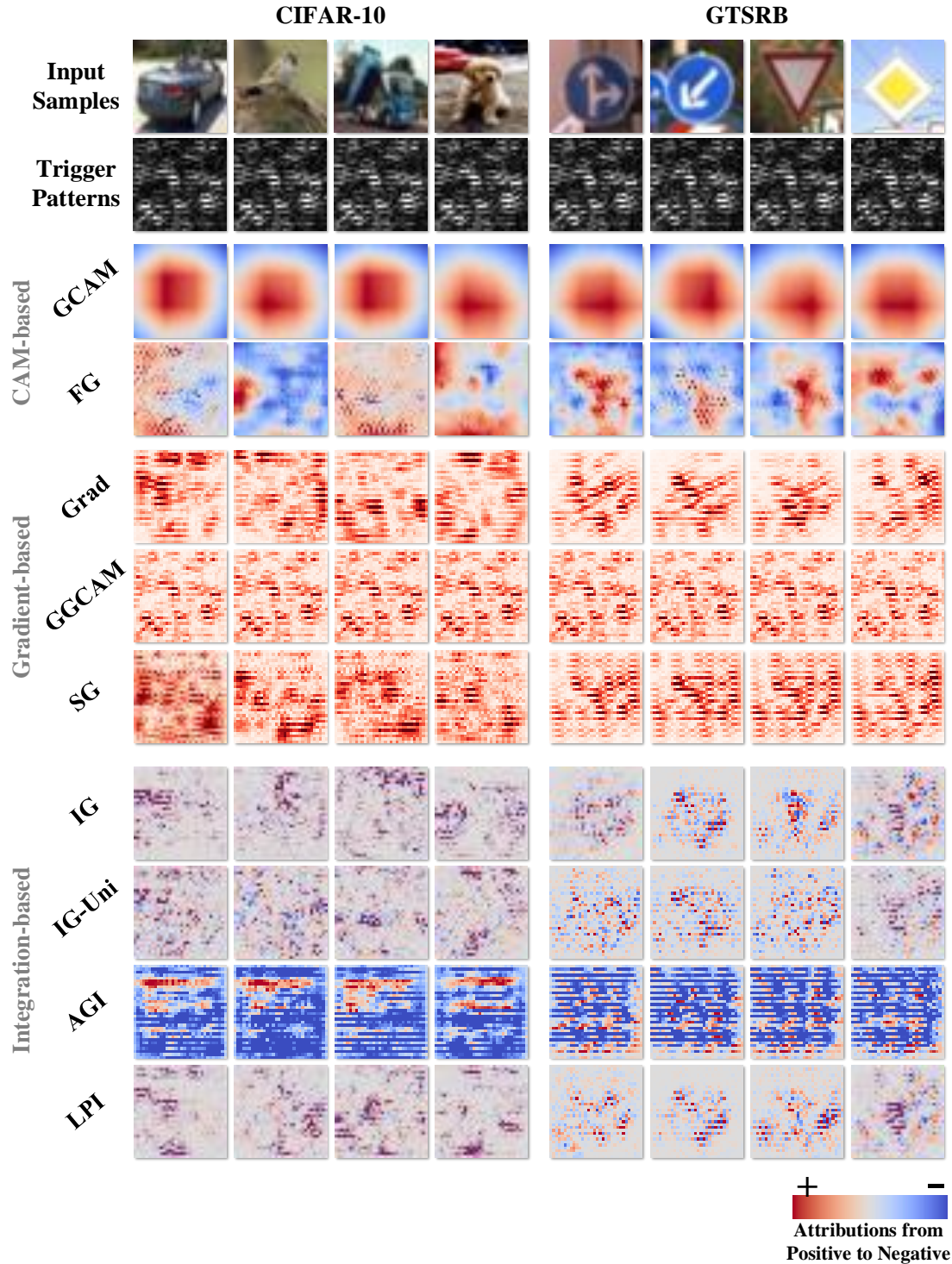


Fig. 24. Visual comparison of attribution methods on CIFAR-10 and GTSRB datasets. Predictions made by ResNet-18 models Trojaned through the ISSBA attack with a trigger visibility of 0.5 are explained using three groups of attribution methods including CAM-based, Gradient-based, and Integration-based methods.

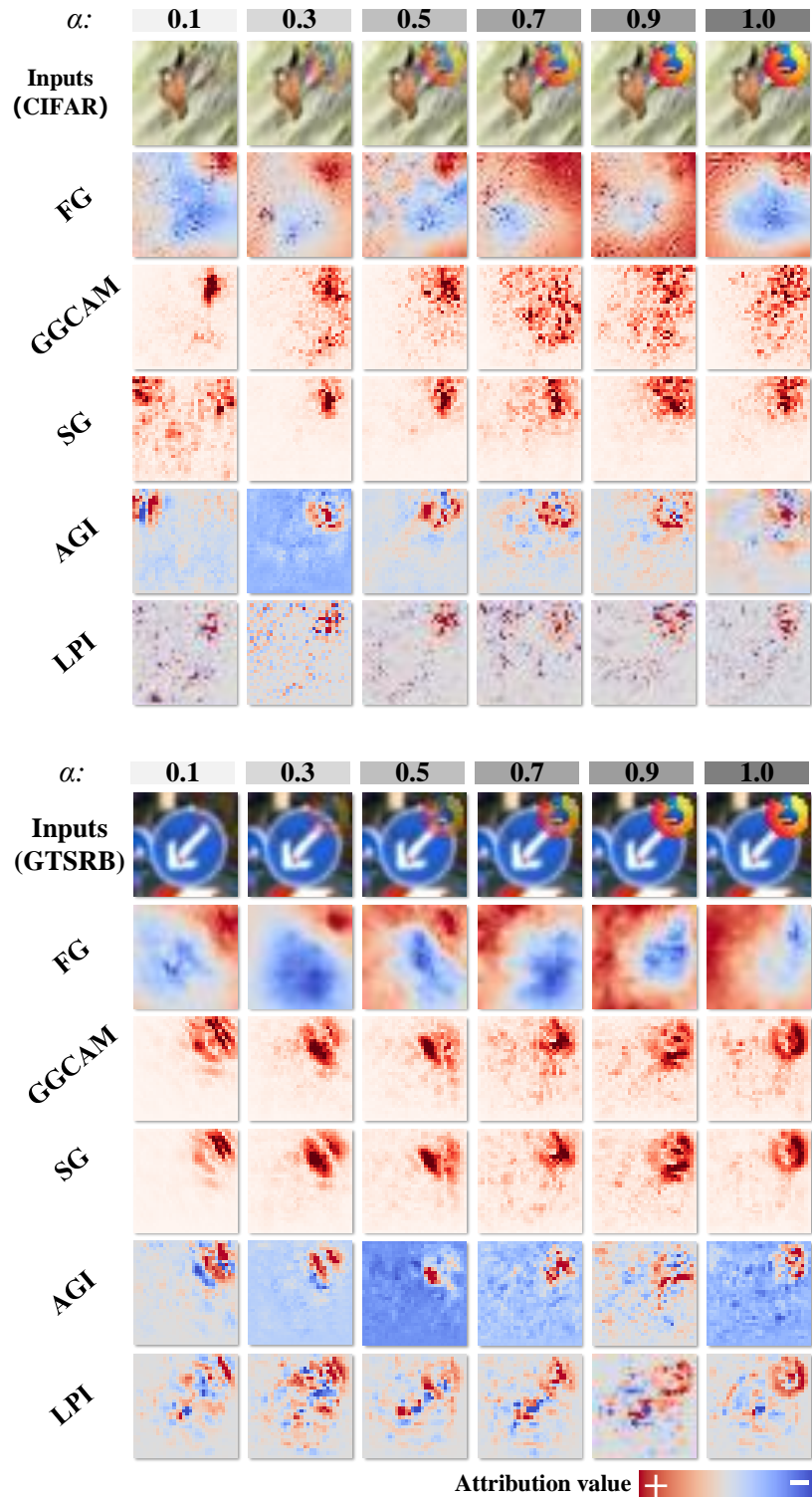


Fig. 25. Visual comparison of attribution methods on CIFAR-10 and GTSRB datasets. Predictions made by ResNet-18 models Trojaned through the Blend attack with triggers of varying visibilities (α) are explained using attribution methods including FG, GGCAM, SG, AGI and LPI.

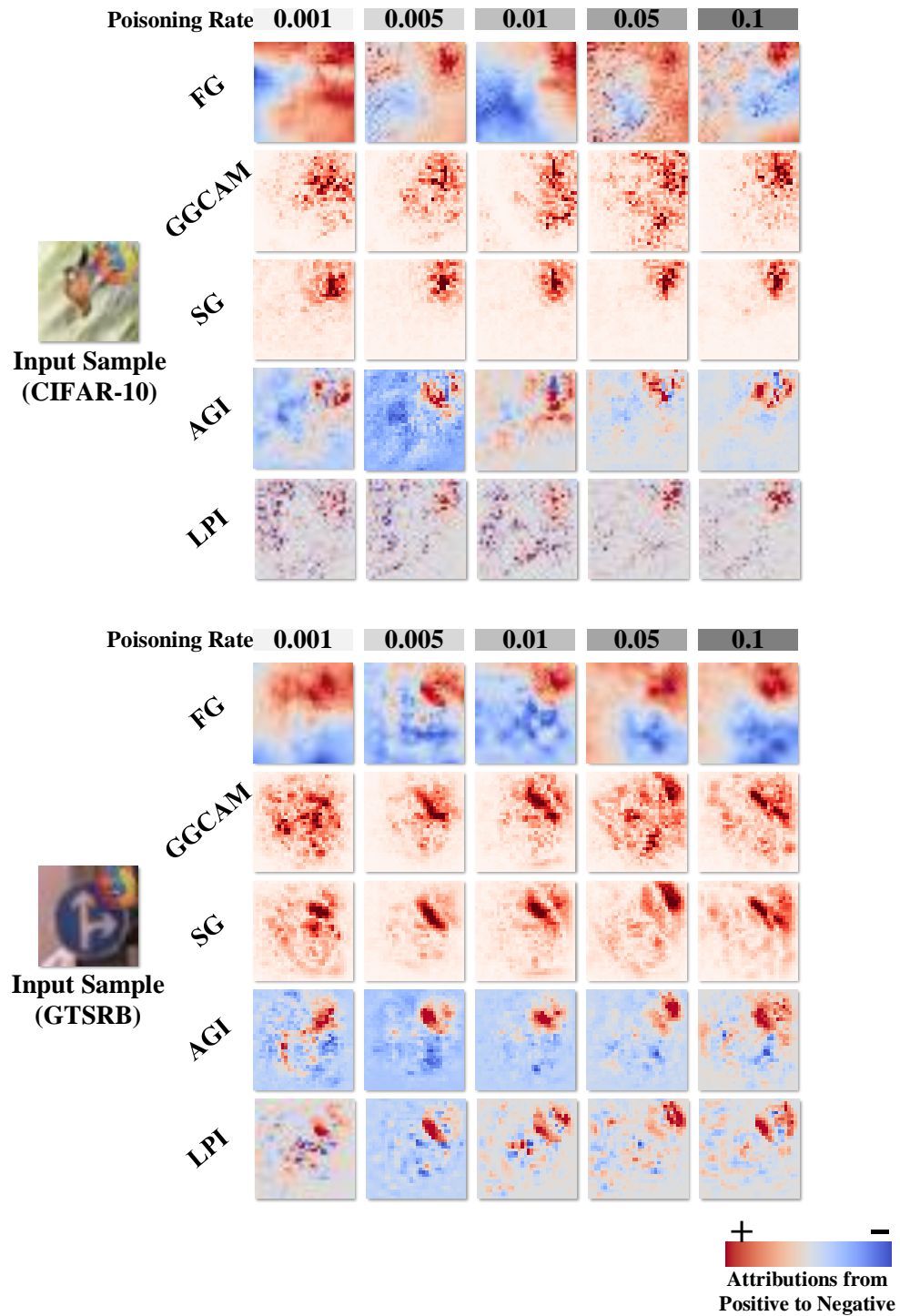


Fig. 26. Visual comparison of attribution methods on CIFAR-10 and GTSRB datasets. Predictions made by ResNet-18 models Trojaned through the Blend attack of different poisoning rates are explained using three groups of attribution methods including FG, GGCAM, SG, AGI and LPI.